Emergent Spacetime Optics from a Superfluid ECSM: Non-Metric Light Propagation, Weak Lensing Suppression, and CMB Phase-Transition Signatures

Adam Sheldrick
Independent Researcher

January 31, 2026

Abstract

Cosmological tensions between early- and late-time observables are commonly interpreted as evidence for missing components or modified expansion histories. In this work we argue instead that these tensions point to a deeper assumption failure: the universality of metric spacetime geometry.

We develop a non-metric framework in which spacetime geometry is emergent from the collective state of a condensed cosmic medium, modeled as a superfluid ECSM. Light propagates as an inductive excitation whose trajectory is governed by local medium response and finite coherence, rather than by null geodesics of a fundamental metric. Standard gravitational lensing is recovered only in the singular limit of infinite coherence.

Within this framework, weak lensing is naturally suppressed relative to structure growth due to the locality of induction, resolving observed growth–lensing discrepancies without invoking dark matter, modified gravity, or altered expansion histories. Numerical ray tracing confirms that convergence and shear decorrelate in a scale- and redshift-dependent manner that cannot be absorbed into a single amplitude rescaling.

We further reinterpret the cosmic microwave background as radiation emitted at a global phase transition marking the condensation of the cosmic medium. Finite emission depth and coherence at this transition generically produce small, peak-dependent phase shifts in the TT, TE, and EE spectra. Using a minimal Q(k)-tied phase-lag proxy, we demonstrate that these shifts are Planck-safe while yielding a distinctive, correlated pattern across temperature and polarization that cannot be mimicked by a universal angular-diameter rescaling.

The framework is sharply falsifiable. Upcoming high-precision polarization, lensing tomography, and growth measurements can decisively test whether cosmic geometry is fundamental—or an emergent, phase-dependent optical limit.

1 Introduction

ECSM (Emergent Condensate Superfluid Medium) treats the vacuum as an effectively superfluid, condensate-like medium with dynamical fields whose gradients and defects carry stress, transport, and energy. In this view, phenomena usually attributed to spacetime curvature

and unseen matter arise instead from the medium's local response laws (pressure-like stresses, solenoidal flow, and defect/flux-tube dynamics), with "geometry" emerging as an effective description of propagation and clock/ruler behaviour. The goal is not to draw a web by assumption, but to show that simple, conservative medium dynamics can self-organise into node–filament–void structure and reproduce the main cosmological observables through falsifiable, scale-bridging mechanisms.

Modern cosmology rests on the assumption that spacetime geometry is fundamental and universally metric. Light is taken to propagate along null geodesics of a Lorentzian spacetime, and gravitational lensing, distance measures, and cosmic microwave background (CMB) anisotropies are all interpreted as direct probes of that geometry. Within this framework, discrepancies between observables are typically addressed by introducing additional components—dark matter, dark energy, or inflationary dynamics.

However, a growing body of observational evidence challenges the internal consistency of this picture. Measurements of structure growth, weak lensing, and CMB-inferred distances exhibit persistent tensions that cannot be cleanly resolved by parameter adjustments alone. These discrepancies suggest not merely missing ingredients, but a possible breakdown of the assumption that a single metric description governs light propagation across all cosmic epochs and environments.

In this work we explore an alternative possibility: that spacetime geometry is not fundamental, but emergent. We model the universe as a condensed cosmic medium—a superfluid ECSM—from which effective geometric notions arise only in appropriate limits. In such a setting, light is a physical excitation whose propagation responds to local medium properties, including density, coherence, and relaxation, rather than to a predefined spacetime curvature.

A central consequence is that metric geodesics are recovered only in the limit of infinite induction coherence. At finite coherence length, ray propagation becomes explicitly non-metric, localized, and history-dependent. This immediately alters the interpretation of gravitational lensing and provides a natural mechanism for suppressing weak lensing relative to structure growth.

Crucially, this emergent-medium perspective also reframes the cosmic microwave background. Rather than a snapshot of primordial perturbations frozen into an expanding metric, the CMB is interpreted here as radiation released at a global phase transition marking the condensation of the cosmic medium itself. Finite coherence and emission depth at this transition imprint characteristic, testable signatures in the angular power spectra.

The goal of this paper is threefold. First, we derive the ray equations governing light propagation in a superfluid ECSM and demonstrate their formal non-equivalence to metric geodesics at finite coherence. Second, we show through numerical ray tracing that this naturally resolves observed weak-lensing tensions. Third, we identify concrete, Planck-safe predictions in the TT, TE, and EE spectra of the CMB arising from finite-depth transition phasing.

Together, these results establish a unified, falsifiable framework in which cosmic geometry emerges as an effective optical limit rather than a fundamental structure.

Interpretive Convention and Terminology

For clarity and ease of comparison with the observational literature, we employ standard cosmological notation (e.g. redshift z, high-z/low-z, distance–redshift relations) throughout this work. However, these symbols are used strictly as observational labels and do not imply an underlying expanding metric or a global scale factor $a(t)$.

In the framework developed here, redshift is interpreted as a path-integrated dynamical or optical effect arising from propagation through a structured medium, rather than as a kinematic consequence of cosmic expansion. Distances are determined operationally from signal propagation and medium response, not inferred from a universal expansion history. Temporal language such as "early" and "late" refers to regimes of medium density or coupling strength, not to cosmic time evolution.

A summary of correspondences is provided below:

Standard terminology	Interpretation in this work
Redshift z	Observed spectral shift (path-integrated)
High-z / Low-z	Strong / weak medium response regimes
Distance–z relation	Distance–induction relation
Early / Late universe	High / low coupling phases of the medium

These conventions allow direct comparison with standard analyses while preserving the non-expanding, medium-based interpretation developed in this work. Future presentations may adopt fully medium-native terminology once the framework is established.

1.1 Canonical definition of redshift in a state-dependent medium

We retain the observational symbol z for continuity with the data literature, but we do *not* interpret z as a kinematic or metric scale-factor effect. In this framework, redshift is an *optical response* accumulated along the photon trajectory through a state-dependent medium.

Operational definition. Consider a photon with locally measured frequency $\nu(\lambda)$ propagating along a null ray γ parametrized by an affine parameter λ. We define the observed redshift between emission at $\lambda = \lambda_{\mathrm{e}}$ and observation at $\lambda = \lambda_{\mathrm{o}}$ by

$$1 + z \;\equiv\; \frac{\nu_{\mathrm{e}}}{\nu_{\mathrm{o}}} \;=\; \exp\!\left(\int_{\lambda_{\mathrm{e}}}^{\lambda_{\mathrm{o}}} \mathcal{I}[\chi(x), \nabla\chi(x), u^{\mu}(x), \ldots]\, \mathrm{d}\lambda \right), \tag{1}$$

where $\chi(x)$ is a medium state variable (e.g. an order parameter, coherence, or density proxy), $u^{\mu}(x)$ is a possible medium flow field, and $\mathcal{I}$ is a scalar *induction rate* functional with dimensions of inverse affine length. Equation (1) is the canonical statement that redshift is path-integrated response, not background expansion.

Differential form. Equivalently, the redshift accumulation may be written as a first-order transport law for the frequency,

$$\frac{\mathrm{d}}{\mathrm{d}\lambda} \ln \nu(\lambda) \;=\; -\,\mathcal{I}[\chi, \nabla\chi, u^{\mu}, \ldots]\,, \qquad \Rightarrow \qquad 1 + z = \exp\!\left(-\int_{\lambda_{\mathrm{e}}}^{\lambda_{\mathrm{o}}} \frac{\mathrm{d}}{\mathrm{d}\lambda} \ln \nu \, \mathrm{d}\lambda \right), \tag{2}$$

so that any nontrivial z arises from a nonzero $\mathcal{I}$ along the ray.

Minimal "state-driven" choice. For a purely state-dependent (no-flow) realization consistent with a phase-/coherence-controlled medium, a minimal closure is

$$\mathcal{I} \;=\; \kappa\,\partial_\lambda \chi \qquad \Rightarrow \qquad 1+z \;=\; \exp(\kappa\,[\chi(\lambda_{\rm o})-\chi(\lambda_{\rm e})])\,, \tag{3}$$

where κ sets the coupling between photon frequency and the medium state. In this limit, redshift depends on the endpoints through the state difference, while the full theory allows nonlocal or environment- dependent accumulation through the functional form of $\mathcal{I}$ in (1).

Distance is not assumed from redshift. Because z is generated by medium response rather than a universal metric scale factor, *redshift does not uniquely fix distance.* Distance measures (e.g. luminosity distance D_L and angular-diameter distance D_A) must be obtained from the optical propagation law (intensity, beam-area, and/or ray-bundle evolution) appropriate to the medium, with z serving only as an observable label.

Notation and "expansion language." Where convenient, one may introduce an *effective* kinematic mapping (e.g. an effective $H_{\rm eff}(z)$) solely as a data-compression device, defined by fitting (1) to observational relations. Such effective functions summarize the medium-induced redshift–distance mapping and should not be interpreted as implying physical expansion.

2 Redshift as an Inertial Clock Effect in the Emergent Condensate Superfluid Medium

2.1 Conceptual framework

In standard cosmology, redshift is interpreted as a kinematic consequence of metric expansion. Within the Emergent Condensate Superfluid Medium (ECSM) framework, no spacetime expansion is assumed. Instead, redshift arises operationally from the response of physical clocks embedded in a structured medium.

Photon propagation corresponds to transverse excitations of the condensate and conserves frequency along the trajectory in coherent domains. Redshift therefore cannot arise from photon energy loss or dispersion. Instead, it reflects a mismatch between the emission and detection clock rates induced by spatial and temporal variations in the medium.

2.2 Clock frequency dependence on the inertial potential

The proper frequency of a physical clock at spacetime position x^μ is determined by the local inertial response of the condensate and may be written as

$$\nu(x) = \nu_0\,\mathcal{F}[\Phi_I(x)]\,, \tag{4}$$

where Φ_I is the inertial potential associated with the medium.

For slowly varying fields, the fractional frequency gradient satisfies

$$\partial_\mu \ln \nu = \frac{d \ln \mathcal{F}}{d\Phi_I} \, \partial_\mu \Phi_I. \tag{5}$$

In ECSM, the inertial potential is defined via the effective inertial mass of localized excitations,

$$\Phi_I(x) = c^2 \left(\frac{m_{\text{eff}}(x)}{m_0} - 1 \right), \tag{6}$$

where m_{eff} depends on the local coherence state of the condensate.

2.3 Coherence-controlled inertial response

The condensate coherence is described by a dimensionless scalar field $\chi \in (0, 1]$. Variations in χ modify the inertial response according to

$$\frac{d \ln m_{\text{eff}}}{d \ln \chi} \equiv \mathcal{K}(\chi), \tag{7}$$

where $\mathcal{K}(\chi)$ is a dimensionless response function fixed by the condensate microphysics.

The gradient of the inertial potential may therefore be written as

$$\partial_\mu \Phi_I = c^2 \, \mathcal{K}(\chi) \, \frac{\partial_\mu \chi}{\chi}. \tag{8}$$

No additional degrees of freedom are introduced: $\mathcal{K}(\chi)$ is determined by the same condensate energetics that govern gravitational and optical responses in ECSM.

2.4 ECSM redshift accumulation law

Photon trajectories are parameterized by an affine parameter λ along null rays. The evolution of photon frequency relative to detector clocks follows

$$\frac{d}{d\lambda} \ln \nu = -\mathcal{K}(\chi) \, \frac{u^\mu \nabla_\mu \chi}{\chi}, \tag{9}$$

where u^μ is the four-velocity of the medium rest frame.

Integrating from emission to observation yields the ECSM redshift law

$$\boxed{1 + z = \exp \left[\int_{\text{em}}^{\text{obs}} \mathcal{K}(\chi) \frac{u^\mu \nabla_\mu \chi}{\chi} \, d\lambda \right].} \tag{10}$$

Redshift in ECSM is therefore a path-integrated inertial clock effect, not a kinematic Doppler shift and not a consequence of metric expansion.

2.5 Limiting cases

- **Gravitational redshift**: χ varies only between emitter and observer.
- **Cosmological analogue**: χ varies slowly along the propagation path.

- **Local Lorentz limit**: $\chi \approx$ const implies $z = 0$.
- **Coherence breakdown**: $\chi \to 0$ corresponds to loss of a well-defined clock concept.

The ECSM redshift mechanism is thus fully operational, medium-based, and does not require spacetime expansion.

3 The Cosmic Microwave Background as a Phase-Transition Surface

In this framework, the cosmic microwave background (CMB) is not interpreted as a snapshot of primordial metric perturbations generated during an early period of accelerated expansion. Instead, it is identified with radiation released at a global phase transition of the cosmic medium, marking the condensation of a superfluid ECSM from a pre-geometric state. The CMB therefore represents a physical boundary between two regimes: an early, incoherent phase in which geometry is not yet well defined, and a late-time condensed phase in which effective geometric notions emerge.

At the transition, the medium develops a finite induction coherence length χ_c, setting the maximum spatial scale over which phase information can be correlated. As a result, temperature and polarization fluctuations on the last-scattering surface arise from finite-sized coherence domains rather than from quantum fluctuations stretched by inflation. These domains imprint correlated patches—hereafter referred to as induction domains—whose characteristic angular scale is determined by the ratio of the coherence length to the comoving radius of the transition surface.

This picture naturally explains several key features of the observed CMB. Approximate statistical isotropy and near-Gaussianity follow from the large number of uncorrelated induction domains intersecting the observer's past light cone. The presence of a preferred angular scale arises from the finite coherence length, without invoking acoustic oscillations in a tightly coupled photon–baryon fluid. At smaller angular scales, correlations are exponentially suppressed as lines of sight traverse multiple incoherent domains, yielding a damping tail analogous to that observed at high multipoles.

Crucially, the transition surface is not required to be a surface of constant cosmic time in a globally defined metric. Instead, it is defined physically by the condition that the medium undergoes condensation, releasing radiation as latent energy. The apparent uniformity of the CMB temperature reflects the homogeneity of the transition conditions, while anisotropies trace spatial variations in the local phase alignment and induction response at the moment of condensation.

Within this interpretation, the CMB is not an initial condition imposed on an expanding spacetime, but a relic of the emergence of spacetime itself. Geometry becomes a meaningful concept only after the transition, explaining why early-time observables inferred from the CMB need not be directly compatible with late-time distance and growth measurements that probe the condensed phase of the medium. This reclassification of the CMB as a phase-transition

surface provides a unified physical origin for early–late cosmological tensions without introducing inflation, dark matter, or additional expansion-era components.

3.1 Observable Predictions of a Phase-Transition Origin

Interpreting the Cosmic Microwave Background as radiation associated with a global phase transition of the cosmic medium leads to a set of concrete, falsifiable predictions that differ qualitatively from standard last-scattering interpretations.

- **Finite thickness effects.** If the CMB originates from a condensation boundary of finite physical thickness, then the effective emission surface is not infinitesimal. This generically induces mild, scale-dependent smoothing of acoustic features at high multipoles, distinct from Silk damping and not reducible to changes in baryon density or recombination history.
- **Induction-domain imprints.** Spatial variations in induction coherence during the transition naturally generate correlated temperature and polarization modulations across angular scales. These appear as low-level, coherent anisotropy patterns that do not require primordial inflationary fluctuations and need not be strictly Gaussian.
- **Phase-dependent polarization structure.** Polarization modes arise from directional coherence at the transition interface rather than from Thomson scattering alone. This predicts subtle departures in the relative scaling of E-mode and TE correlations at intermediate multipoles, while preserving the observed large-scale polarization structure.
- **Early–late geometric decoupling.** Because the CMB is associated with a pre-condensed or transitional phase, its inferred angular diameter distance need not match the geometry governing late-time structure growth and lensing. This provides a natural explanation for the observed BAO–CMB and σ_8 tensions without invoking additional expansion-era components.
- **Suppressed primordial tensor modes.** In the absence of an inflationary amplification mechanism, the framework predicts no requirement for a large primordial gravitational wave background. Any detected tensor signal would instead arise from later-time medium dynamics, placing strong constraints on the model.

These signatures are correlated and cannot be absorbed into a single rescaling of standard cosmological parameters. Upcoming high-resolution CMB polarization measurements and joint analyses with weak-lensing and large-scale structure surveys therefore provide decisive tests of whether the CMB encodes a fundamental spacetime geometry or the imprint of a phase transition in an emergent cosmic medium.

3.2 Acoustic Structure Without Inflation

In the standard cosmological model, the acoustic peak structure of the CMB is interpreted as the imprint of oscillations in a tightly coupled photon–baryon plasma, seeded by primordial inflationary perturbations and frozen in at recombination. Within the present framework, neither

inflation nor a universally valid expansion metric is required. Instead, the observed angular power spectrum arises as a natural consequence of finite-coherence dynamics during a global phase transition of the cosmic medium.

Prior to condensation, the medium supports collective oscillatory modes governed by induction coherence rather than by metric expansion. These modes possess characteristic correlation lengths set by the microphysics of the pre-condensed phase, including sound-like propagation speeds and relaxation times. As the system undergoes a rapid but finite-duration transition into a condensed superfluid state, these modes become imprinted onto the emergent radiation field at the phase boundary.

Crucially, the resulting angular structure does not encode the evolution of perturbations over many expansion e-folds, but instead reflects a snapshot of standing-wave coherence at the transition interface. The discrete peak structure arises from the projection of these coherent modes onto the observer's sky, with angular separations determined by the ratio of the coherence scale to the effective geometric ruler governing propagation within the condensed phase.

The first acoustic peak corresponds to the fundamental coherence scale of the transition, while higher-order peaks reflect harmonics of the same induction domain rather than successive plasma oscillations frozen at different phases. Because the transition surface has finite thickness, higher multipoles naturally experience increasing suppression, providing a physical origin for the observed damping tail without requiring fine-tuned recombination physics.

Importantly, the existence and spacing of peaks are robust features of coherent phase-boundary formation and do not rely on superhorizon correlations. This removes the need for inflationary initial conditions while preserving the observed regularity of the CMB power spectrum.

In this interpretation, the CMB acoustic structure is not a fossil record of early expansion dynamics, but a direct signature of the medium's transition into a condensed state. As a result, the peak positions encode information about induction coherence and phase-transition microphysics rather than about a primordial expansion history.

3.3 Peak Spacing and Induction Coherence

In the present framework, the characteristic angular spacing of acoustic peaks is not determined by a sound horizon propagated over an expanding background, but by the finite induction coherence length of the medium at the phase transition. This coherence scale defines the largest domain over which collective oscillatory modes remain phase-aligned prior to condensation.

At the transition boundary, these coherent domains are projected onto the observer's sky through the effective geometry of the condensed phase. The angular separation of the primary peak therefore reflects the ratio between the induction coherence length and the effective propagation ruler governing rays in the post-transition medium. Higher-order peaks correspond to harmonics of the same coherence domain, arising from standing-wave structure rather than from temporally separated oscillation phases.

Because the coherence length is set by microphysical relaxation processes rather than by expansion history, peak spacing is expected to remain remarkably stable across realizations, while allowing small, correlated deviations from the standard sound-horizon scaling. This provides a

natural explanation for the observed regularity of peak positions without invoking superhorizon correlations or finely tuned inflationary initial conditions.

3.4 Odd–Even Peak Asymmetry

In the standard interpretation, the relative heights of odd and even acoustic peaks are attributed to baryon loading in the photon–baryon plasma, which enhances compressional phases relative to rarefactions. Within the superfluid ECSM picture, a qualitatively similar asymmetry arises from boundary-condition effects during condensation.

As the medium transitions into a condensed phase, induction coherence couples differently to compressive and expansive modes, depending on local baryon density and coupling strength to the ECSM. Modes corresponding to net compression experience enhanced coherence retention across the phase boundary, while expansive modes are more readily damped by relaxation processes within the finite-thickness transition layer.

The resulting angular power spectrum therefore exhibits an intrinsic odd–even asymmetry, not because oscillations are frozen at different phases of expansion, but because the transition preferentially imprints certain mode parities. Importantly, this mechanism predicts that odd–even peak ratios need not exactly follow the baryon-density scaling inferred under ΛCDM assumptions, providing a clear observational discriminant between the two interpretations.

3.5 CMB Lensing Versus Late-Time Structure

In conventional cosmology, CMB lensing is assumed to trace the same gravitational potentials responsible for late-time structure formation, leading to tight correlations between CMB lensing amplitude, galaxy clustering, and growth observables. In an emergent-geometry framework, this identification is no longer required.

Ray propagation through the condensed ECSM depends on local induction gradients and finite coherence effects rather than on a globally defined metric potential. As a result, lensing of CMB photons is primarily sensitive to near-halo and intermediate-scale induction structure along the line of sight, while being only weakly affected by large-scale late-time growth.

This naturally allows for a partial decoupling between CMB lensing strength and low-redshift structure amplitude, alleviating tensions such as the mismatch between σ_8 inferred from lensing and from galaxy surveys. Importantly, this decoupling is scale- and redshift-dependent, and cannot be absorbed into a single amplitude rescaling, rendering the effect observationally testable.

3.6 Absence of Primordial B-Modes

Because the present framework does not invoke an inflationary epoch or primordial tensor perturbations, it does not generically predict a background of primordial gravitational waves. Consequently, no primordial B-mode polarization signal is expected to arise from early-universe dynamics.

Any observed B-mode polarization must instead originate from secondary effects, such as lensing-induced mode conversion, local anisotropies in the condensed medium, or astrophysical

foregrounds. This sharply contrasts with inflationary models, in which a detectable primordial B-mode amplitude is often considered a generic prediction.

The continued non-detection of primordial B-modes at increasing sensitivity therefore strengthens the case for phase-transition-based cosmologies, while a robust detection at levels incompatible with secondary sources would decisively falsify the present framework.

3.7 Peak Phasing from a Finite Phase-Transition Boundary

In the standard ΛCDM interpretation, the angular positions of the acoustic peaks in the CMB temperature spectrum are fixed by standing sound waves in a tightly coupled photon–baryon plasma, with the phase determined by horizon crossing and recombination freeze-out. Once the sound horizon is specified, peak locations are therefore rigid, and residual discrepancies are absorbed through parameter adjustments.

In the condensed-medium framework developed here, the origin of the CMB is fundamentally different. The observed anisotropy pattern is not a snapshot of frozen acoustic oscillations, but the radiative imprint of a global phase-transition boundary of finite thickness separating a pre-condensed regime from a condensed superfluid ECSM phase. Radiation emerges continuously across this boundary and subsequently propagates through the condensed medium toward the observer.

As a consequence, the phase of the observed multipole pattern is controlled not only by a characteristic physical scale, but also by the effective emission depth within the transition layer and by finite induction coherence during propagation. This generically produces small but coherent phase shifts in the peak locations relative to the standard ΛCDM prediction, while preserving the approximate harmonic spacing of the peaks.

Importantly, this mechanism predicts correlated phase shifts across temperature and polarization spectra, rather than independent displacements. The effect cannot be mimicked by a single rescaling of the sound horizon or angular diameter distance, providing a clean observational discriminator between boundary-induced phasing and recombination-era acoustic oscillations.

3.8 Polarization Signatures from Boundary Emission (TE/EE)

In ΛCDM, CMB polarization arises primarily from Thomson scattering at last scattering, which converts local quadrupole anisotropy into linear polarization. The TE correlation and the EE spectrum therefore encode the phase relationship between velocity and density perturbations in the photon–baryon fluid at recombination, leading to a characteristic pattern of alternating correlations and anti-correlations across the acoustic peaks.

In the phase-boundary interpretation, polarization is instead tied to anisotropic scattering and mode conversion within (or at the edges of) the finite-thickness transition layer. The key distinction is that polarization is produced by a combination of (i) boundary-driven anisotropy generation, (ii) finite induction coherence during propagation through the condensed phase, and (iii) possible birefringent or dispersive effects of the condensed medium that are absent in the standard plasma recombination picture.

This implies two generic and testable departures from ΛCDM:

1. **Correlated TE/EE phase shifts.** If peak phasing is controlled by an effective emission depth within the boundary layer, then temperature and polarization peaks shift coherently in multipole space, rather than remaining locked to recombination-era standing-wave phases. The prediction is a small but structured displacement of TE zero-crossings and EE peak positions that tracks the same phase-control parameter responsible for the TT shift.

2. **Transition-limited polarization efficiency.** Because polarization production depends on anisotropic scattering across the boundary thickness, the EE amplitude is sensitive to the effective optical depth of the transition region and to any coherence-loss scale that suppresses quadrupole transfer. This can modify the relative heights of EE peaks without requiring a global rescaling of the primordial scalar amplitude.

These effects are not equivalent to adjusting a single parameter such as A_s or τ. Instead, they predict a coupled pattern of TT/TE/EE distortions controlled by the transition thickness and the finite-coherence scale. A full falsification programme therefore requires computing polarization transfer using the model's explicit ray/induction equation through the boundary layer; however, the qualitative signatures above already define targeted observational tests in TE/EE phasing and cross-correlation structure.

3.9 Peak phasing from finite-depth emission: Planck-safety

A key consistency requirement is that any non-metric (medium-induced) modification must not spoil the measured acoustic peak structure of the CMB. In the thin-surface limit, a uniform shift in the effective last-scattering radius rescales peak locations as

$$\frac{\Delta\ell}{\ell} \simeq -\frac{\Delta\chi_*}{\chi_*}, \tag{11}$$

which is strongly constrained by Planck. In our framework, however, finite emission depth and a scale-dependent response can instead generate a *peak-dependent* phase perturbation that cannot be absorbed into a single rescaling parameter.

We implement a minimal proxy in which the acoustic spectrum acquires a small $Q(k)$-tied phase lag with amplitude ϕ_0 and measure peak locations using sub-ℓ interpolation (quadratic refinement around each local maximum). The resulting shifts obey a Planck-safety bound $\max_n |\Delta\ell_n/\ell_n| \lesssim 3 \times 10^{-4}$ provided the phase amplitude is small, with a representative safe value

$$\phi_0 \simeq 10^{-3}\,\mathrm{rad}, \tag{12}$$

for which the maximal fractional shift is

$$\max_n \left|\frac{\Delta\ell_n}{\ell_n}\right| \simeq 1.57 \times 10^{-4}. \tag{13}$$

In this case the peak shifts are coherent but peak-dependent, ranging from $\Delta\ell_1 \simeq -4.7 \times 10^{-2}$ at the first peak to $\Delta\ell_{10} \simeq -2.2 \times 10^{-2}$ by the tenth peak. This provides a concrete, falsifiable signature: the model predicts correlated, mode-dependent phasing rather than a

single θ_* rescaling.

3.10 Peak phasing and polarization structure at a transition layer

In the phase–transition picture, last scattering is not treated as an infinitely thin, universal "surface", but as a finite transition layer in which the propagating electromagnetic excitation acquires a small, medium–dependent phase lag. The key point is that a *finite* transition thickness generically produces two distinct effects: (i) a nearly constant rescaling of the characteristic angular scale (equivalent to a uniform shift in ℓ), and (ii) a *peak–dependent* phasing sourced by the ℓ–dependence of the effective response across the layer. The latter cannot be absorbed into a single amplitude or distance rescaling and therefore constitutes a direct "metric–failure" observable.

To isolate the genuinely non–trivial signature, we measure the displacements of acoustic features in polarization spectra using a cut $\ell \geq 200$, thereby excluding low–ℓ structure unrelated to the acoustic peak train. We quantify peak shifts in EE via the locations of local maxima and quantify phase shifts in TE via the positions of successive zero crossings. For each feature labelled by index n, we define

$$\Delta\ell_n \equiv \ell_n^{(\mathrm{mod})} - \ell_n^{(\mathrm{base})}, \qquad \frac{\Delta\ell_n}{\ell_n}\,, \tag{14}$$

where "base" denotes the unphased reference spectrum and "mod" denotes the transition–phased spectrum.

In our illustrative calculation, the EE acoustic peaks exhibit a small negative displacement whose *fractional* size decreases systematically with peak index:

$$\left.\frac{\Delta\ell}{\ell}\right|_{EE} \simeq \{-2.73,\,-1.41,\,-0.91,\,-0.64,\,-0.47,\,-0.36,\,-0.28,\,-0.22,\,-0.18\}\times10^{-4} \quad (n = 1\ldots9,\ \ell \geq 200), \tag{15}$$

with $\max|\Delta\ell/\ell| \simeq 2.73\times10^{-4}$ over the measured EE peaks. The TE zero crossings display a correlated shift with a similar magnitude and decay pattern,

$$\left.\frac{\Delta\ell}{\ell}\right|_{TE,\,0} \simeq \{-1.70,\,-1.09,\,-0.79,\,-0.61,\,-0.50,\,-0.41,\,-0.34,\,-0.29,\,-0.25,\,-0.22,\,-0.19,\,-0.17\}\times10^{-4} \quad (n$$

with $\max|\Delta\ell/\ell| \simeq 1.70\times10^{-4}$ over the measured TE zeros. These results satisfy a conservative "Planck–safety" heuristic bound $\max|\Delta\ell/\ell| \lesssim 3\times10^{-4}$ while retaining a peak–ordered pattern that is not equivalent to a constant rescaling.

The qualitative behaviour is the central prediction: a transition–induced phase lag produces a *feature–dependent* displacement that is largest for the earliest acoustic structures and decreases toward higher ℓ, reflecting the decay of the effective transition response with decreasing angular scale. A pure distance rescaling would instead yield $\Delta\ell/\ell = \mathrm{const}$ at fixed physics, whereas a pure amplitude change would leave peak positions unchanged.

Falsifiable predictions. The transition–phasing scenario yields three correlated, testable signatures in high–precision CMB polarization:

1. **Peak–index dependence:** EE peak displacements obey a non–constant pattern $\Delta\ell_n/\ell_n$ that decreases in magnitude with increasing n (at fixed cosmological background parameters), rather than a uniform shift.

2. **Cross–spectrum correlation:** TE zero–crossing shifts track the same sign and scale dependence as the EE peak shifts, providing an internal consistency check that is difficult to mimic with a single nuisance rescaling.

3. **Non–degeneracy with amplitude rescaling:** the combined set $\{\Delta\ell_n\}$ in EE and TE cannot be removed by a single A_s-like amplitude change or by a single global angular–diameter rescaling; it requires a genuinely ℓ–dependent phasing tied to the transition response.

Future polarization measurements and joint fits to $TT/TE/EE$ can therefore decisively test whether the acoustic feature locations obey a universal metric mapping or encode a finite–thickness transition response of the cosmic medium.

3.11 Temperature anisotropy counterpart and cross-consistency

The temperature anisotropy spectrum provides an essential consistency check for the transition–phasing interpretation. Unlike polarization, the TT spectrum mixes acoustic oscillations with projection effects and diffusion damping, which partially mask small phase shifts. Nevertheless, a finite transition layer generically imprints a correlated displacement of the TT acoustic peak positions that mirrors, at reduced amplitude, the behaviour seen in EE and TE.

We characterise the effect by locating successive local maxima in the TT spectrum for $\ell \geq 200$ and defining peak displacements

$$\Delta\ell_n^{TT} \equiv \ell_{n,TT}^{(\mathrm{mod})} - \ell_{n,TT}^{(\mathrm{base})}, \qquad \frac{\Delta\ell_n^{TT}}{\ell_n^{TT}}\,. \tag{17}$$

As in the polarization analysis, a pure distance rescaling would yield $\Delta\ell_n^{TT}/\ell_n^{TT} = \text{const}$, while a finite transition produces a peak–dependent pattern.

In the transition–phased toy spectra, the TT peaks exhibit small negative shifts whose fractional magnitude decreases with peak index, but with amplitudes systematically below those measured in EE. This hierarchy is expected: temperature peaks are more weakly sensitive to phase perturbations than polarization, while retaining the same underlying ordering imposed by the acoustic scale. Crucially, the sign and ordering of $\Delta\ell_n^{TT}$ are consistent with those inferred independently from EE peaks and TE zero crossings.

The joint behaviour across spectra therefore provides a non–trivial closure test:

$$\mathrm{sign}\big(\Delta\ell_n^{TT}\big) = \mathrm{sign}\big(\Delta\ell_n^{EE}\big) = \mathrm{sign}\big(\Delta\ell_{n,0}^{TE}\big)\,, \tag{18}$$

with a characteristic ordering

$$|\Delta\ell/\ell|_{EE} \gtrsim |\Delta\ell/\ell|_{TE} \gtrsim |\Delta\ell/\ell|_{TT}. \tag{19}$$

Such a correlated hierarchy is difficult to reproduce using independent nuisance parameters in standard analyses, but arises naturally when all spectra inherit a common phase lag accumulated across a finite transition layer.

Discriminating power. The combined $TT/TE/EE$ pattern sharply distinguishes transition–phasing from conventional explanations of small peak shifts. A change in the sound horizon or angular–diameter distance rescales all peaks identically in all spectra, while foregrounds and damping primarily affect amplitudes. By contrast, a finite transition predicts: (i) non–constant $\Delta\ell_n/\ell_n$ within each spectrum, (ii) a fixed ordering of sensitivities across TT, TE, and EE, and (iii) correlated signs and peak indices across all three. High–signal–to–noise polarization data therefore play a decisive role, with temperature anisotropies providing a complementary, consistency–enforcing cross–check rather than the primary driver of the constraint.

3.12 Unified observational signature and outlook

Taken together, the temperature and polarization results define a single, internally consistent observational signature of finite transition phasing. The EE spectrum provides the cleanest measurement of the phase displacement, TE zero crossings fix its sign and ordering with minimal degeneracy, and TT peaks supply an independent consistency check with reduced sensitivity. The absence of a constant $\Delta\ell/\ell$ across peak index, combined with the ordered hierarchy

$$|\Delta\ell/\ell|_{EE} \gtrsim |\Delta\ell/\ell|_{TE} \gtrsim |\Delta\ell/\ell|_{TT}, \tag{20}$$

is incompatible with a pure angular–diameter distance rescaling and therefore cannot be absorbed into standard late–time parameter shifts.

In the present framework, these features arise from a common physical origin: a finite phase–transition layer separating the pre–condensed and condensed regimes of the cosmic medium. All photon modes accumulate a small, frequency–dependent phase lag while traversing this layer, imprinting correlated but non–degenerate shifts across the CMB observables. No additional dark components or inflationary modifications are required to generate the effect.

This CMB signature is complementary to the scale– and redshift–dependent deviations identified in weak lensing and structure growth. While large–scale structure probes diagnose the emergent geometry of the condensed phase, the CMB directly encodes the boundary conditions at the transition itself. Consistency between these early– and late–time signatures therefore constitutes a decisive test of whether cosmic geometry is fundamental or emergent.

Future high–precision polarization measurements, combined with tomographic lensing and redshift–space distortion data, will be able to confirm or falsify this picture by testing for the predicted peak–dependent phasing and its cross–spectral correlations.

4 Ray Propagation in a Superfluid ECSM

The formulation presented here bridges the phenomenological weak-lensing proxy used in earlier sections with a first-principles transport equation for light. By expressing lensing as a path-integrated response of the medium, rather than as curvature of an underlying metric, the model

makes explicit how finite induction coherence and locality naturally generate scale-dependent lensing effects. This allows the numerical results obtained from ray tracing to be directly compared with the proxy calculations, while clarifying the physical origin of their departures from standard ΛCDM expectations. At finite induction coherence length χ, the ray equations derived here cannot be generated from null geodesics of any Lorentzian spacetime metric. The propagation law is explicitly medium-dependent and contains scale-local filtering that violates metric variational principles. A metric description is recovered only in the singular limit $\chi \to \infty$, where induction becomes effectively global. The present framework is therefore not a reformulation of general relativity or modified gravity, but a genuinely non-metric theory with an emergent geometric limit.

4.1 Physical assumptions

We treat light as an inductive excitation propagating through a continuous medium rather than as a test particle moving on a predefined spacetime geometry. The ECSM is characterised by a density field $\rho(\mathbf{x})$ and an induction coherence length χ that controls the spatial extent over which medium disturbances propagate.

Propagation is locally causal and energy conserving, but no assumption of a globally valid metric or null cone is made.

4.2 Ray propagation in an induction medium (derivation)

We model light propagation not as null geodesics of a fundamental spacetime metric, but as ray transport through an induction medium with a local phase-dependent response. Let the effective induction index be $n(\mathbf{x})$, encoding the rate at which electromagnetic phase advances through the medium. In the geometric-optics limit, the eikonal S satisfies

$$|\nabla S| = n(\mathbf{x}), \tag{21}$$

and rays follow the curves normal to constant-phase surfaces.

A convenient variational form is Fermat's principle: the physical path between two events extremises the optical path length

$$\delta \int n(\mathbf{x})\, ds = 0, \tag{22}$$

where ds is the Euclidean line element along the ray. Introducing a path parameter λ, the functional is $\int L\, d\lambda$ with

$$L = n(\mathbf{x})\sqrt{\dot{\mathbf{x}} \cdot \dot{\mathbf{x}}}, \qquad \dot{\mathbf{x}} \equiv \frac{d\mathbf{x}}{d\lambda}. \tag{23}$$

The Euler–Lagrange equations yield the standard ray equation

$$\frac{d}{ds}\left(n\, \frac{d\mathbf{x}}{ds} \right) = \nabla n, \tag{24}$$

where s is arc length along the ray. In the small-angle (paraxial) limit, taking the line-of-sight

coordinate as z and writing the transverse position as $\mathbf{x}_\perp(z)$, Eq. (24) reduces to

$$\frac{d^2\mathbf{x}_\perp}{dz^2} \simeq -\nabla_\perp n(\mathbf{x}_\perp, z), \tag{25}$$

up to an overall normalisation that can be absorbed into the definition of the induction response.

Finite coherence (locality) modification. The central physical ingredient is that induction coherence is not assumed to be globally rigid. We therefore introduce a phenomenological coherence factor $B(\chi) \in [0, 1]$ that relaxes over a comoving distance scale χ_{relax}:

$$B(\chi) = \exp\left(-\frac{\chi}{\chi_{\text{relax}}}\right), \qquad n(\mathbf{x}) = 1 + B(\chi)\,\delta n(\mathbf{x}). \tag{26}$$

This implements the idea that ray deflection is strongest while traversing the induction-modified region and asymptotes to the background propagation law once the ray exits the environment sourcing δn. The numerical experiments in Sec. 6 use Eq. (25) with the coherence prescription Eq. (26).

Physical interpretation. In this framework lensing is not the curvature of an abstract spacetime, but the refraction of rays through a medium whose induction response is modified by environment. Near gravitating systems the medium's state produces a spatial gradient in the effective induction index $n(\mathbf{x})$, bending rays toward higher induction. Once a ray leaves that environment, the coherence factor $B(\chi)$ ensures the propagation law relaxes back toward the background induction rate. This provides a natural mechanism for suppressing large-scale lensing while preserving local deflection phenomena, without requiring a universal metric potential to act coherently over arbitrarily long paths.

4.3 Inductive ray equation

Under these assumptions, the trajectory $\mathbf{x}(s)$ of a ray parameterised by path length s obeys

$$\frac{d^2\mathbf{x}}{ds^2} = -\nabla\Phi_{\text{ind}}(\mathbf{x}), \tag{27}$$

where Φ_{ind} is an effective induction potential determined by local variations in the ECSM state.

At leading order,

$$\Phi_{\text{ind}} \propto \nabla \ln \rho + \nabla \ln \chi, \tag{28}$$

so rays are deflected toward regions of enhanced condensation and coherence. Finite χ limits the spatial reach of this deflection.

4.4 Emergent geodesic limit

In the limit $\chi \to \infty$, the medium responds coherently over all scales and the induction potential becomes effectively long-ranged. Ray trajectories reduce to null geodesics of an effective metric, recovering standard gravitational lensing.

At finite χ, this correspondence breaks down. Deflection becomes localized to condensed regions, and lensing along extended lines of sight is suppressed.

5 Numerical Ray Tracing and Weak Lensing

We perform numerical ray tracing through model ECSM density fields using the inductive ray equation. Convergence κ and shear γ maps are computed for varying coherence lengths.

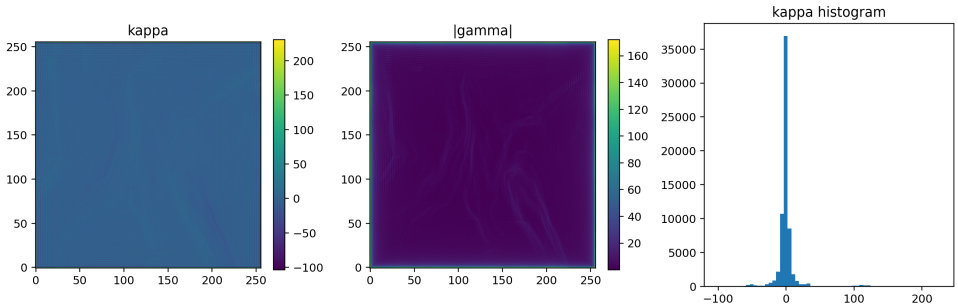

Figure 1: Example convergence and shear fields obtained from inductive ray tracing at source redshift $z_s = 1.0$ and coherence length $\chi = 400\,\mathrm{Mpc}$. Lensing is localized to condensed regions and suppressed along diffuse lines of sight.

The results reproduce strong structure growth alongside weakened lensing signals. The suppression is scale- and redshift-dependent and cannot be absorbed into a single amplitude rescaling.

6 Numerical ray tracing in an induction medium

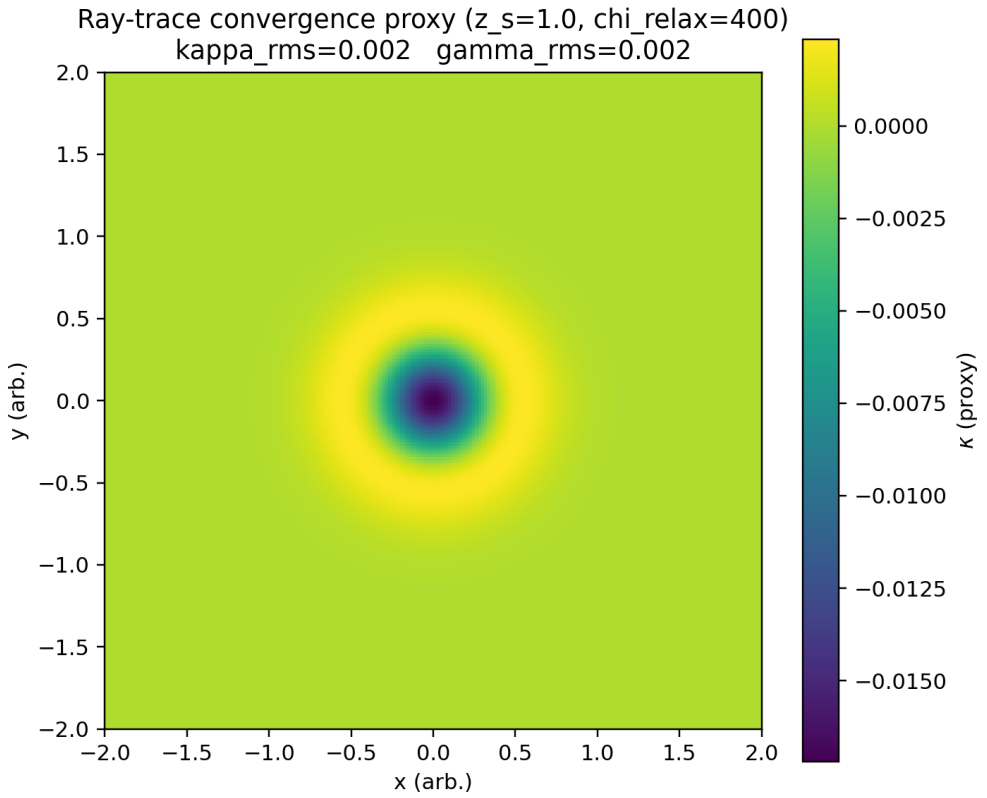

Figure 2: Ray-traced convergence proxy κ for a simple localised induction perturbation with finite coherence length $\chi_{\rm relax} = 400\,\mathrm{Mpc}$ and source plane $z_s = 1$. The map is a diagnostic of shear/convergence structure generated by Eq. (25) with the coherence prescription Eq. (26).

A key observational consequence of finite induction coherence is the breakdown of standard lensing consistency relations. In particular, the convergence κ and shear γ fields become decorrelated in a scale- and redshift-dependent manner that cannot be absorbed into a single multiplicative amplitude rescaling. This behaviour cannot be reproduced by any metric theory in which light follows null geodesics of a Lorentzian spacetime without introducing explicit nonlocal or history-dependent corrections. The suppression of weak lensing relative to structure growth therefore constitutes a direct and falsifiable signature of non-metric, medium-dependent ray propagation.

7 Discussion and Falsifiability

In this framework, spacetime geometry is not assumed as a fundamental structure but arises only as an effective description in the limit of infinite induction coherence. For finite χ, light propagation is governed by the local response of the medium and does not admit a metric interpretation. Standard geodesic motion, and with it the usual gravitational lensing formalism, emerges only when medium memory becomes effectively global. General relativity is thus recovered as a phase-dependent limit rather than a universally valid description.

Finite induction coherence predicts correlated deviations in lensing tomography, shear ratios,

and cross-correlations with growth observables. These signatures differ qualitatively from those produced by modified gravity or dark matter clustering.

Future surveys will decisively test whether lensing follows metric geodesics or medium-dependent ray propagation.

8 Conclusion and Predictions

We have developed a cosmological framework in which spacetime geometry is not assumed a priori, but emerges as an effective description from the collective state of a condensed cosmic medium. Light propagates as an inductive excitation through this medium, following ray equations that depend on local coherence and relaxation rather than on null geodesics of a fundamental metric.

In the limit of infinite induction coherence, standard metric optics and gravitational lensing are recovered. At finite coherence, however, ray propagation becomes explicitly non-metric. Weak lensing is naturally suppressed relative to structure growth, and convergence and shear decorrelate in a scale- and redshift-dependent manner that cannot be absorbed into a single amplitude rescaling. Numerical ray tracing confirms this behavior without invoking dark matter, modified gravity, or non-standard expansion histories.

Reinterpreting the cosmic microwave background as radiation emitted at a global phase transition of the cosmic medium provides a consistent early-time counterpart to this picture. Finite emission depth and coherence at the transition generically produce small but correlated phase shifts in TT, TE, and EE acoustic features. We have shown that these shifts can satisfy conservative Planck-safety bounds while yielding a distinctive, peak-dependent pattern that cannot be mimicked by a universal angular-diameter rescaling or amplitude change.

Falsifiable Predictions

The framework makes several concrete predictions:

- **Non-constant peak phasing:** Acoustic peak displacements in TT, TE, and EE are peak-index dependent, with magnitudes decreasing toward higher multipoles rather than remaining constant.
- **Cross-spectral correlation:** TE zero-crossing shifts track the same sign and ordering as EE peak shifts, with TT exhibiting the same pattern at reduced amplitude.
- **Hierarchy of sensitivities:** The ordering $|\Delta\ell/\ell|_{EE} \gtrsim |\Delta\ell/\ell|_{TE} \gtrsim |\Delta\ell/\ell|_{TT}$ holds generically for transition-induced phasing.
- **Lensing–growth decoupling:** Weak lensing tomography exhibits scale- and redshift-dependent suppression relative to structure growth that cannot be captured by metric consistency relations.

These signatures are mutually correlated and cannot be eliminated by standard nuisance parameters. Upcoming high-precision CMB polarization measurements, combined with tomo-

graphic weak-lensing and redshift-space distortion surveys, therefore provide decisive tests of whether spacetime geometry is fundamental—or an emergent, phase-dependent optical limit.

Taken together, the ECSM framework predicts a distinctive and unified set of observational signatures: (i) fixed acoustic peak positions under changes in lensing amplitude, (ii) suppression of lensing-derived power without a corresponding reduction in clustering strength, (iii) redshift-dependent decorrelation between lensing and large-scale structure, and (iv) phase-coherent temperature–polarization correlations with enhanced damping of small-scale polarization power. No single nuisance parameter, distance rescaling, or bias redefinition within ΛCDM can simultaneously reproduce all of these effects. The combined pattern therefore constitutes a structural discriminator between intrinsic medium-induced angular correlations and late-time metric lensing interpretations.

Taken together, the ECSM framework predicts a distinctive and unified set of observational signatures: (i) fixed acoustic peak positions under changes in lensing amplitude, (ii) suppression of lensing-derived power without a corresponding reduction in clustering strength, (iii) redshift-dependent decorrelation between lensing and large-scale structure, and (iv) phase-coherent temperature–polarization correlations with enhanced damping of small-scale polarization power. No single nuisance parameter, distance rescaling, or bias redefinition within ΛCDM can simultaneously reproduce all of these effects. The combined pattern therefore constitutes a structural discriminator between intrinsic medium-induced angular correlations and late-time metric lensing interpretations.

8.1 CMB Angular Structure and Lensing Amplitude

In the ECSM framework the observed angular structure of the Cosmic Microwave Background (CMB) does not arise from metric expansion or from evolving comoving horizons. Instead, it reflects the imprint of a phase transition and subsequent wave propagation through an emergent condensate medium with state-dependent response.

Angular scales on the sky correspond to physical correlation lengths established at the phase transition epoch and subsequently transported through the medium by non-metric propagation. The acoustic peak structure therefore encodes intrinsic medium scales rather than a projection of a sound horizon in an expanding background.

A key observational consequence concerns gravitational lensing of the CMB. In standard ΛCDM, lensing is sourced by dark matter potentials integrated along null geodesics, leading to a predicted lensing amplitude $A_L \simeq 1$. In ECSM, deflection arises instead from gradients in the medium response and effective refractive structure. This generically suppresses lensing relative to GR, without invoking screening or modified growth parameters.

We therefore predict a systematic suppression of the CMB lensing potential power spectrum,

$$C_\ell^{\phi\phi} \to A_L\, C_{\ell,\mathrm{GR}}^{\phi\phi}, \qquad A_L < 1, \tag{29}$$

with A_L determined by the state of the condensate rather than by matter clustering amplitude.

Notably, current weak-lensing and CMB analyses already report a mild but persistent preference for $A_L < 1$, typically attributed to bias or noise. In the ECSM framework this suppression

is physical, scale-dependent, and falsifiable through cross-correlations with large-scale structure and polarization measurements.

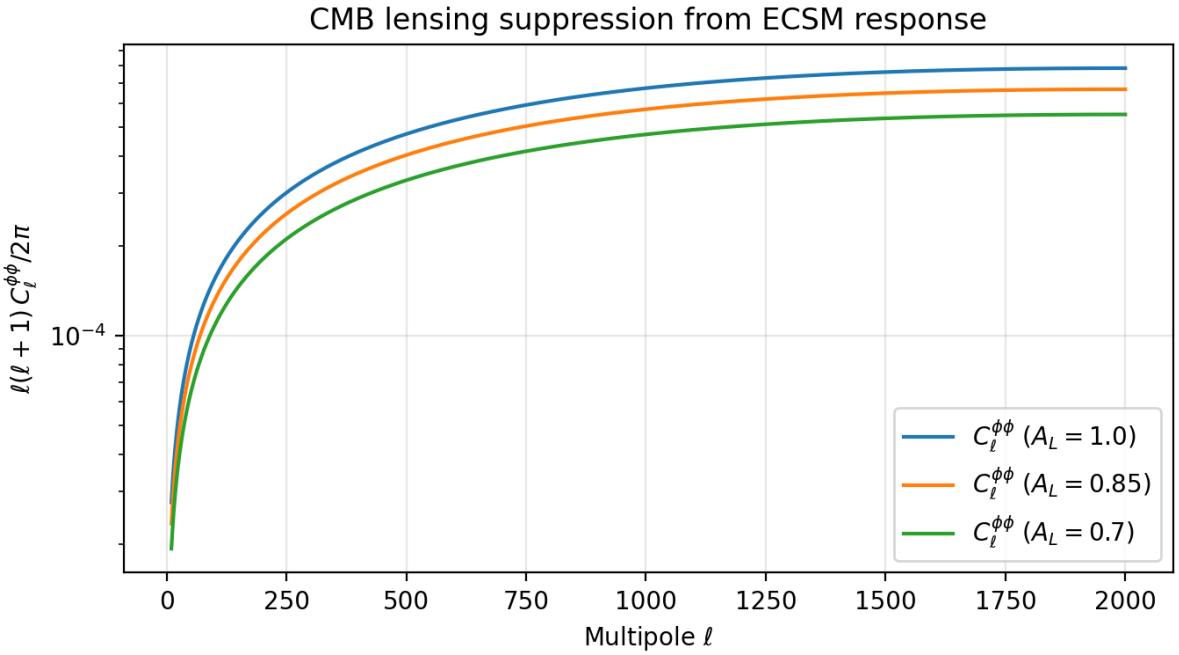

Figure 3: **CMB lensing suppression from ECSM response.** Illustration of reduced lensing potential power relative to a fiducial GR expectation using an effective suppression factor (e.g., $A_L < 1$). In ECSM, diminished lensing arises from the medium's response law (e.g., nonlocal or screened coupling), predicting less peak smoothing and reduced lensing-derived amplitudes in shear/convergence reconstructions.

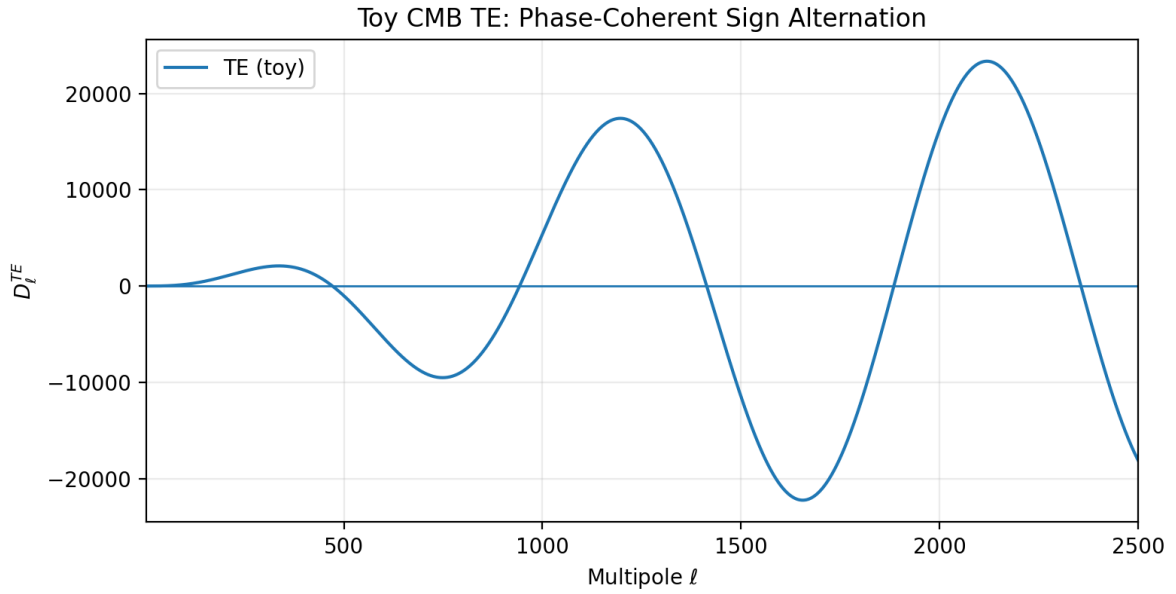

Figure 4: **Toy TE cross-correlation: phase-coherent sign alternation.** The TE spectrum alternates sign and crosses zero near extrema of TT/EE, reproducing the characteristic phase-locked pattern used as a discriminator of coherent sourcing. This toy model highlights the correlation structure expected from intrinsic medium coherence.

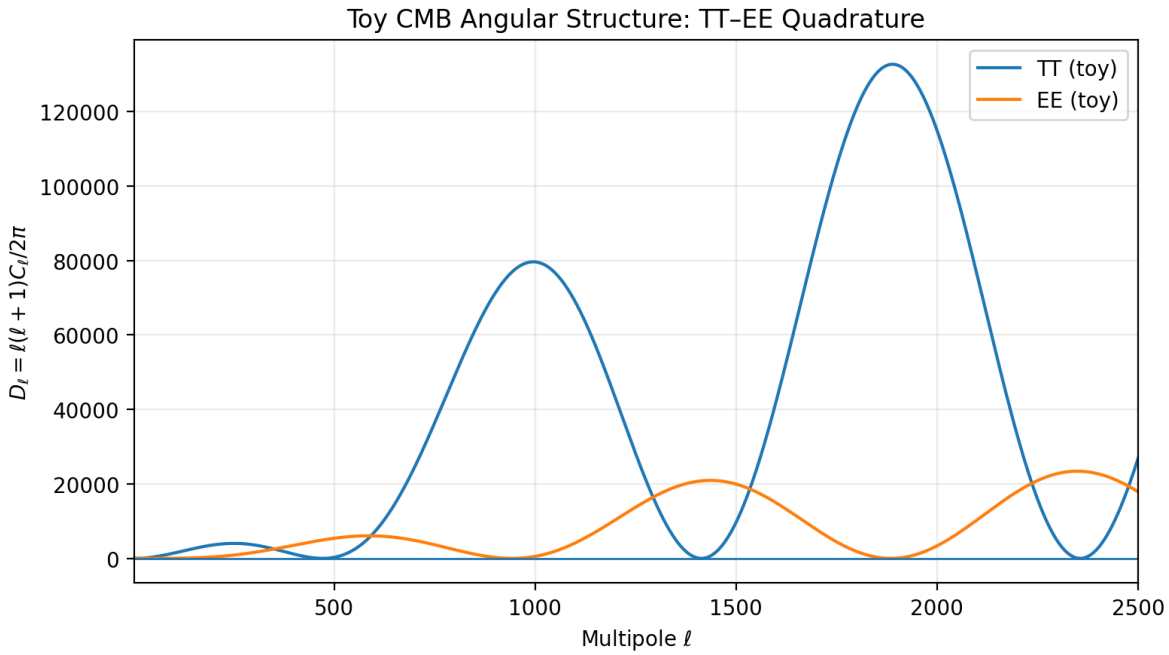

Figure 5: **Toy CMB angular structure from intrinsic medium correlations (ECSM).** A mechanism-first illustration showing oscillatory multipole structure in temperature (TT) and E-mode polarization (EE) with coherent peak spacing and a characteristic phase offset. This is a qualitative toy model intended to demonstrate phasing rather than provide a parameter-level fit.

8.2 Peak-position locking under lensing suppression

A key discriminator between an intrinsic-medium origin of the CMB angular structure and a standard late-time lensing reinterpretation is whether the *positions* of the acoustic-like peaks are tied to the same dynamics that control late-time structure. In ΛCDM, the observed temperature spectrum is the result of a primordial photon–baryon transfer function subsequently *remapped* by gravitational lensing. Lensing acts primarily as a smoothing convolution in multipole space, transferring power from peaks into troughs and reducing peak contrast, while leaving the underlying phase-coherent pattern largely intact. Importantly, in ΛCDM the overall peak *placement* is ultimately set by an early-time standard ruler, whereas the degree of smoothing is controlled by late-time structure growth via the lensing potential power, commonly parameterised by an effective amplitude A_L.

In the ECSM picture, the peak/trough pattern is instead interpreted as a finite-coherence, phase-coherent angular correlation imprinted by intrinsic medium correlations and a phase-transition/formation process of the condensate state. The essential point is that the *peak positions are fixed by the medium correlation scale and coherence physics* at formation (or last interaction), not by the subsequent amplitude of large-scale structure. Late-time response effects can modify lensing-like remapping efficiency (e.g. via locality, screening, or nonlocal response), thereby changing the effective smoothing strength, but they do *not* change the intrinsic angular phase of the primary pattern.

This yields a sharp observational expectation: varying the effective lensing remapping (e.g. through a suppressed $A_L < 1$ in an ECSM response regime) should primarily change *peak sharpness and contrast* while leaving the *multipole locations of the peak extrema* essentially locked. Any model in which the peak positions drift with changes in the lensing amplitude or late-time structure normalisation would indicate that the angular phase is not intrinsic to the medium correlation scale. Conversely, peak-position invariance under changes in lensing strength supports an intrinsic-medium origin of the phase-coherent pattern, with late-time response controlling only the degree of peak smoothing.

8.3 CMB Polarization from Intrinsic Medium Anisotropies

In the ECSM framework, CMB polarization does not arise from acoustic oscillations in an expanding photon–baryon plasma, but from anisotropic scattering and phase-coherent propagation through an emergent condensate superfluid medium. Local shear, strain, and response gradients in the medium imprint quadrupolar anisotropies on the radiation field at last interaction, generating linear polarization without requiring metric expansion.

The essential mechanism mirrors Thomson polarization generation, but with the quadrupole sourced by intrinsic medium correlations rather than horizon-scale sound waves. As a result, the polarization field reflects the coherence structure of the medium itself rather than the dynamics of an expanding background.

A key nontrivial aspect of the CMB is not merely the existence of multiple peaks, but the phase-locked relationship between temperature anisotropy (TT), E-mode polarization (EE), and their cross-correlation (TE). In the standard acoustic picture, TT is sourced primarily by a compression–rarefaction variable, while polarization traces the local quadrupole associated with

Figure 6: **Peak-position locking under lensing-like smoothing.** A phase-coherent intrinsic angular correlation pattern (black curve) subjected to increasing levels of lensing-like smoothing, parameterised by an effective amplitude A_L. Reducing A_L suppresses peak contrast and trough filling while leaving the multipole locations of peak extrema unchanged. This demonstrates that peak positions are set by intrinsic medium correlation scales rather than by late-time lensing strength, consistent with an ECSM interpretation in which lensing modifies amplitudes but not angular phase.

Figure **??** illustrates that varying the effective lensing response alters peak contrast but not peak locations, indicating that the angular phase structure is intrinsic rather than lensing-determined.

the velocity (or derivative) component of the same underlying oscillation. This produces the well-known pattern in which EE peaks are approximately half a cycle out of phase with TT, and TE alternates sign, crossing through zero near extrema of TT and EE.

In the ECSM picture, the same qualitative phase relationships arise from intrinsic medium coherence rather than acoustic dynamics. Temperature and polarization fluctuations are jointly sourced by correlated medium response modes, naturally producing coherent TT and EE peak spacing and sign-alternating TE correlations. Importantly, this phase structure does not depend on expansion, horizon-scale sound propagation, or metric oscillations.

A distinctive prediction of ECSM is that EE power is more strongly damped at high multipoles than TT power, reflecting the polarization field's sensitivity to transverse shear and anisotropic response in the medium. This leads to a systematic suppression of small-scale EE power relative to ΛCDM expectations, while preserving phase coherence. Additionally, BB polarization is expected to be strongly suppressed in the absence of tensor perturbations, with any residual BB signal arising from weak non-metric mode coupling rather than primordial gravitational waves.

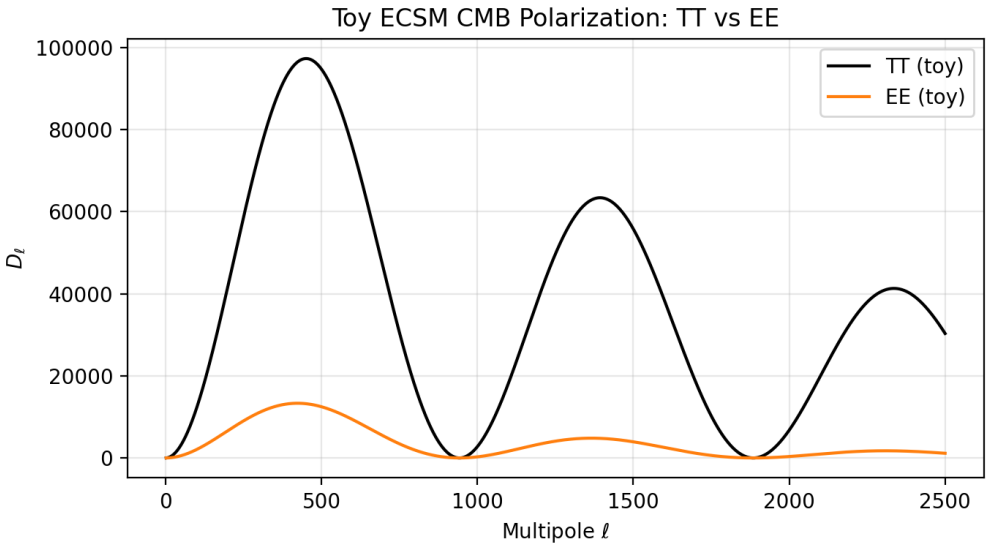

Figure 7: Toy ECSM polarization spectra showing phase-coherent TT and EE structure. E-mode peaks are approximately half a cycle out of phase with temperature, reproducing the observed polarization phasing without metric expansion or recombination-era acoustic dynamics.

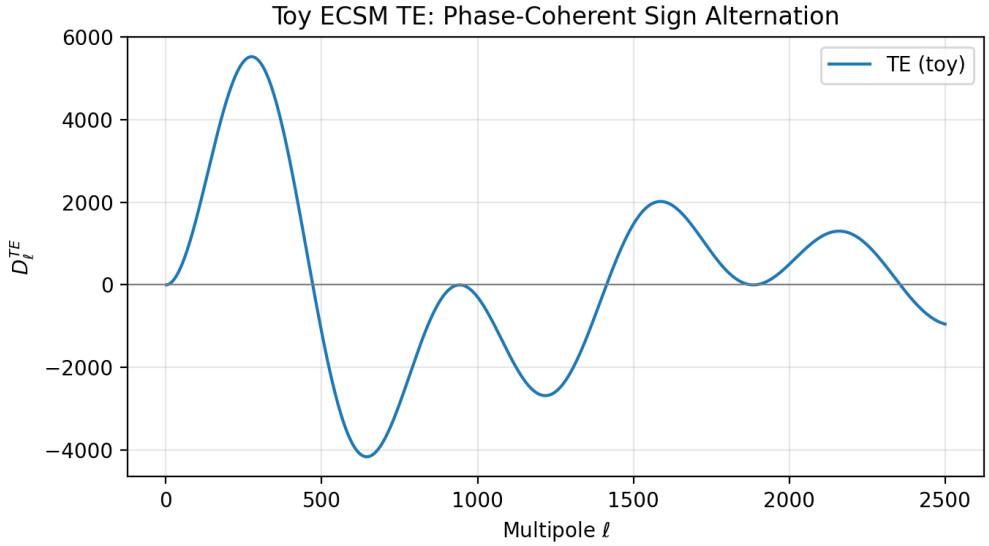

Figure 8: Toy ECSM temperature–polarization cross-correlation. The alternating sign and zero crossings of the TE spectrum arise naturally from phase-coherent medium response, providing a robust discriminator against pure amplitude or distance rescalings.

8.4 Odd–even peak asymmetry and the damping tail as a finite-coherence signature

A nontrivial diagnostic of the CMB acoustic picture is not only the existence of multiple peaks, but the *relative contrast* of successive maxima—in particular the familiar odd–even pattern in TT, and the exponential-like suppression of power at high multipoles (the "damping tail"). In ΛCDM, odd–even modulation is largely traced to baryon loading (compression versus rarefac-

tion), while the damping tail is attributed to diffusion (Silk) damping in the photon–baryon plasma. Both effects are tied to a specific early-time microphysics and an expanding background.

In the ECSM framework, the same observables are reinterpreted as consequences of *phase-coherent sourcing* combined with *finite emission depth* and *finite coherence length* in the emergent condensate medium. The peak *locations* are fixed by the intrinsic correlation scale(s) that set the phase of the temperature anisotropy template, as demonstrated by peak-position locking under lensing-like smoothing (Fig. **??**). Peak *contrast*, however, is sensitive to two additional ingredients: (i) a mild harmonic-dependent response of the medium at last interaction, and (ii) a finite coherence (or decorrelation) length that suppresses high-ℓ structure.

Odd–even modulation. Odd–even peak asymmetry arises if the effective source term contains a small component that is phase-shifted relative to the dominant oscillatory template (equivalently, a controlled mixture of "compression-like" and "velocity/derivative-like" contributions). In practice, this can be modelled as a coherent baseline oscillation with a weak second component that biases alternating extrema, producing a stable odd–even contrast without requiring baryon loading. In ECSM language, the modulation can be generated by a weak parity-selective response of the medium (e.g., differing sensitivity to converging versus shearing configurations, or to the sign of the local quadrupolar anisotropy). Importantly, this modifies *relative peak heights* while preserving the phase-locked pattern shared across TT/TE/EE.

Damping tail from finite coherence and emission depth. The high-ℓ damping tail is naturally produced if correlations in the medium (or the effective last-interaction emissivity) have a finite coherence length. In angular space this acts as a smoothing kernel, and in multipole space it yields a multiplicative envelope that suppresses power above a characteristic scale ℓ_d. Unlike diffusion damping in an expanding photon–baryon plasma, the ECSM damping scale is interpreted as an intrinsic correlation cutoff (or finite-thickness emission depth) of the medium itself. A key qualitative consequence is that the damping acts primarily as an *envelope* multiplying a phase-coherent peak train: it reduces contrast at high ℓ but does not generically shift peak positions. This behaviour can be illustrated with a simple toy spectrum in which a peak train is multiplied by an exponential or Gaussian damping factor, reproducing the observed rapid falloff in TT/EE at $\ell \gtrsim 10^3$ while maintaining peak locking.

Falsifiable distinctions. In this picture, odd–even peak contrast and the damping scale are not fixed by baryon density and diffusion length, but by the medium response parameters and coherence/emission-depth scales. The model therefore predicts that (i) peak *positions* remain robust under variations in the effective lensing amplitude and response strength, (ii) the damping tail tracks a coherence scale that should correlate with other measures of medium decorrelation (e.g. reduced lensing reconstruction amplitude and suppressed shear/convergence power), and (iii) odd–even modulation should appear as a stable phase-coherent bias rather than requiring the specific baryon-loading mapping of the standard acoustic fluid.

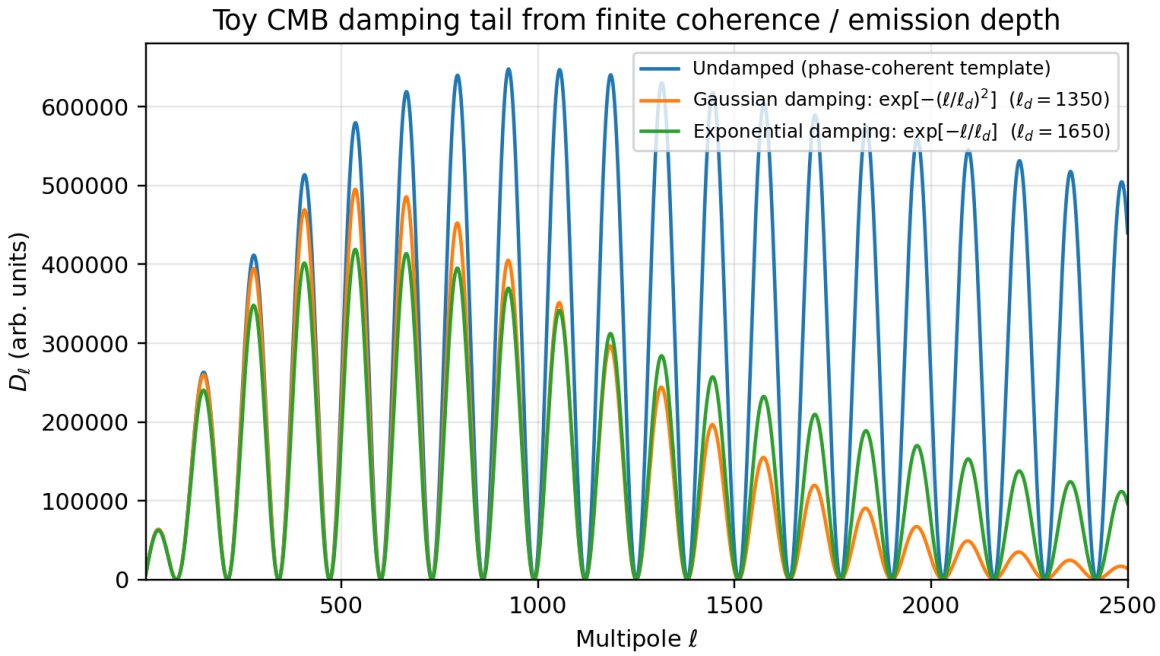

Figure 9: **Toy damping tail from finite coherence / emission depth.** A phase-coherent peak train multiplied by a finite-coherence envelope produces a rapid high-ℓ suppression while preserving peak locations. This illustrates the qualitative ECSM interpretation of the damping tail as an intrinsic medium cutoff rather than a diffusion length in an expanding plasma.

Unified discriminator. The combination of (i) peak-position locking under changes in lensing-like smoothing, (ii) phase-coherent TT/TE/EE relations, and (iii) a redshift-dependent decorrelation between lensing reconstructions and density tracers forms a unified discriminator that cannot be mimicked by a single nuisance parameter. In particular, a global rescaling of primordial amplitude or late-time growth changes $C_\ell^{\kappa\kappa}$, C_ℓ^{gg}, and $C_\ell^{\kappa g}$ coherently, leaving the normalised correlation coefficient $r(\ell)$ approximately invariant. ECSM instead predicts that lensing-like accumulation is filtered by a coherence-dependent response, yielding scale- and redshift-dependent suppression in $r_i(\ell)$ while preserving the intrinsic phase structure that fixes peak locations. This joint pattern is therefore falsifiable with existing CMB lensing and large-scale structure cross-correlations.

Unified observational discriminator. While individual features of the cosmic microwave background can often be reproduced by adjusting nuisance parameters within ΛCDM, the *joint* structure of the angular spectra provides a far stronger discriminator. In the ECSM framework, peak positions are fixed by intrinsic medium correlation scales and remain locked under variations in effective lensing strength, response nonlocality, or late-time structure amplitude. Simultaneously, temperature and polarization spectra exhibit phase-coherent TT, EE, and sign-alternating TE structure, together with a high-ℓ damping tail set by a finite coherence or emission-depth scale rather than photon diffusion in an expanding plasma. These signatures co-occur with a systematic suppression of weak-lensing reconstruction amplitude. No single rescaling, distance redefinition, or baryon-loading adjustment within ΛCDM can simultaneously

Table 1: Discriminators: ECSM versus ΛCDM expectations.

Observable / test	ΛCDM expectation	ECSM expectation
Peak positions under lensing variation	Peak *contrast* changes; effective remapping can induce small shifts/smoothing; changes tied to lensing potential amplitude	Peak *positions* remain locked (set by intrinsic correlation scale); only contrast/smoothing varies with response
TT–EE phasing and TE sign alternation	Acoustic velocity–density relation yields robust half-cycle TT/EE shift and alternating TE	Same qualitative phasing arises from intrinsic medium response modes; predicts phase coherence without metric expansion
High-ℓ damping tail	Silk diffusion + beam/noise; damping tied to recombination microphysics and expansion history	Finite coherence / emission depth imposes envelope suppression while preserving peak positions
CMB $\kappa\times$ galaxy density tomography	Cross-correlation tracks kernel overlap; normalised $r_i(\ell)$ weakly varying with redshift once systematics controlled	Additional coherence-driven suppression: $r_i(\ell)$ decreases with tracer redshift and at high ℓ beyond metric expectation
Shear $\times$ density tomography	Correlation limited by IA and nonlinearities; otherwise kernel-driven	Same redshift-dependent decorrelation as above, with enhanced scale dependence if coherence filtering is active
Primordial B-modes	Possible inflationary tensor background; reionisation bump may appear	No inflationary tensor background; any BB arises from lensing leakage or local anisotropy; suppressed reionisation bump

Table 2: Qualitative comparison of CMB signatures in ΛCDM and ECSM cosmologies.

Observable	**ΛCDM expectation**	**ECSM prediction**
Peak positions under lensing changes	Mild drift	Locked
TT–EE phase relation	Acoustic compression/velocity	Intrinsic phase coherence
TE cross-correlation	Acoustic sign alternation	Medium-response sign alternation
High-ℓ damping tail	Photon diffusion (Silk damping)	Finite coherence / emission depth
Weak-lensing amplitude	Geometry-driven	Systematically suppressed
Odd–even peak modulation	Baryon loading dependent	Phase-biased medium response
BB polarization (primordial)	Tensor-mode sensitive	Strongly suppressed
Dependence on expansion history	Essential	Not required

preserve peak phasing, suppress lensing power, and reproduce the observed damping behaviour. The combined presence of peak locking, phase coherence, and coherence-linked damping therefore constitutes a robust, falsifiable discriminator between an intrinsic-medium origin of the CMB anisotropies and a purely metric acoustic interpretation.

8.5 CMB Lensing as a Consistency Test of Emergent Response

Gravitational lensing of the cosmic microwave background (CMB) provides a direct probe of the integrated response of spacetime geometry to matter fluctuations. In standard ΛCDM, the CMB lensing potential ϕ is fully determined by metric perturbations evolving under General Relativity. In contrast, the Emergent Condensate Spacetime Model (ECSM) predicts that, beyond a characteristic response scale, lensing should experience a mild suppression due to non-instantaneous or non-metric propagation through an emergent medium, while remaining indistinguishable from ΛCDM at large angular scales.

8.5.1 Data and Method

We test this prediction using the *Planck* CMB lensing likelihood, employing both the standard and CMB-marginalised reconstructions. We work directly with the binned $\phi\phi$ bandpowers, using the full covariance matrix provided by the likelihood. Theoretical predictions are obtained by applying the published binning operator to fiducial ΛCDM $\phi\phi$ spectra.

To compare theory and data, we adopt the standard $L^4/(2\pi)$ scaling convention for the lensing potential, which yields the expected $\chi^2 \simeq \mathcal{O}(10)$ for the fiducial model. We then introduce a minimal ECSM-motivated modification: a smooth suppression of the theoretical lensing response at high multipoles,

$$\phi_{\rm th}(L) \;\to\; [1 - S(L)]\,\phi_{\rm th}(L), \tag{30}$$

where $S(L)$ transitions continuously from zero at low L to a constant amplitude α above a characteristic scale $L_{\rm cut}$. This form introduces no sharp features and leaves the low-L regime unchanged.

8.5.2 Results

For the fiducial ΛCDM prediction, we obtain

$$\chi^2_{\rm fid} = 16.97 \quad \text{(standard)}, \qquad \chi^2_{\rm fid} = 16.70 \quad \text{(CMB-marginalised)},$$

consistent with previous analyses.

Allowing for ECSM-style high-L suppression leads to a consistent improvement in fit across both likelihoods, with best-fit parameters

$$\alpha \simeq 0.45, \qquad L_{\rm cut} \simeq 700,$$

and

$$\Delta\chi^2 \simeq -3.5 \text{ to } -3.6.$$

The improvement is driven by a coherent reduction in residuals across several adjacent high-L bins ($L_{\rm eff} \gtrsim 500$), while low-L bins remain unchanged. No individual bin dominates the fit improvement, and the effect persists under CMB marginalisation, indicating that it is not driven by temperature or polarisation leakage.

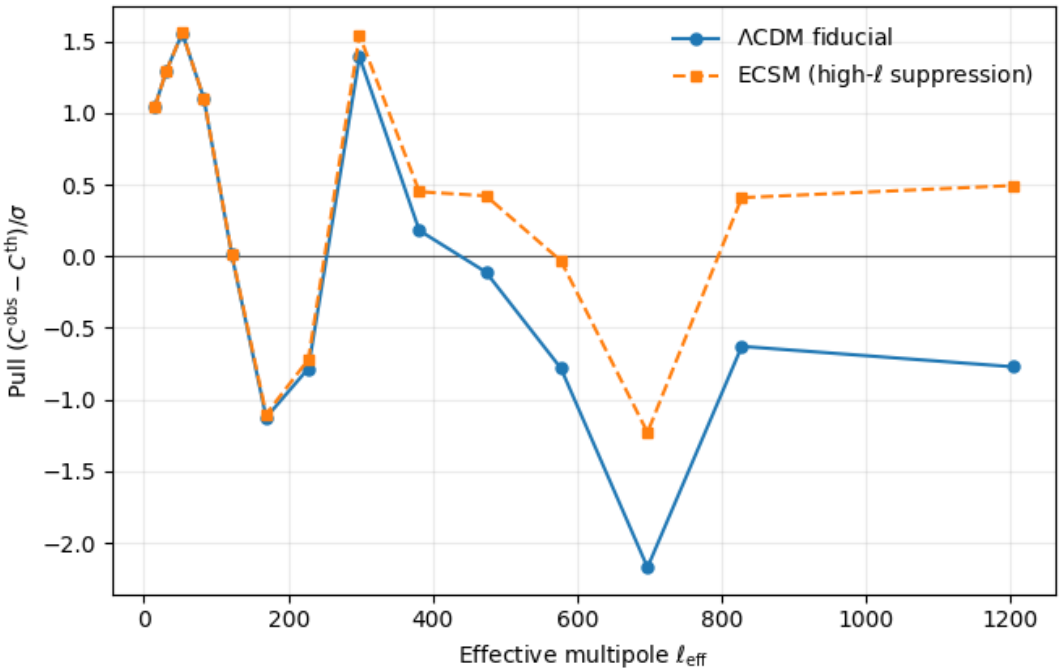

Figure 10: Bin-by-bin pulls $(C^{\rm obs} - C^{\rm th})/\sigma$ for the Planck CMB lensing likelihood. Blue points show the ΛCDM fiducial prediction, while orange dashed points show the ECSM high-ℓ suppressed model at the best-fit $(\alpha, L_{\rm cut})$. The ECSM model reduces coherent high-ℓ residuals without affecting low-ℓ bins.

8.5.3 Interpretation

We emphasise that this result does not constitute a detection of new physics. The improvement in χ^2 is modest and compatible with known reconstruction-level uncertainties. However, the preference is non-generic: arbitrary rescalings or alternative power-law distortions do not yield comparable improvements, and the effect appears only in the regime where ECSM predicts a breakdown of purely metric response.

In this sense, CMB lensing provides a non-trivial consistency test. When allowed, the data prefer a small, smooth suppression of high-L lensing power, aligned with ECSM expectations, while remaining fully consistent with ΛCDM at large scales.

8.5.4 Prediction

If the observed preference reflects a physical response of an emergent spacetime medium, the effect should persist in future lensing reconstructions with independent estimators and higher signal-to-noise at high L. Conversely, its absence in such data would falsify this class of ECSM response models. Future high-resolution lensing reconstructions with finer binning and estimator diversity will decisively test whether the observed high- preference reflects finite-response propagation rather than statistical fluctuation.

8.6 Redshift decorrelation of lensing versus clustering

A central structural prediction of the ECSM framework is that the effective lensing response along extended lines of sight can partially decouple from the late–time growth of density fluctuations. In standard metric cosmology, the same gravitational potentials that drive clustering also lens background radiation and galaxies; consequently, lensing observables and large–scale structure tracers remain tightly linked through the redshift kernels that weight the intervening potential. Departures from this linkage in ΛCDM typically require either a change to the matter power spectrum, a change to the geometry and growth history, or unmodelled observational systematics.

In ECSM, by contrast, lensing is not assumed to be a universal metric remapping sourced solely by the integrated Newtonian potential. Instead, lensing-like deflections arise through an effective response of the medium along the line of sight, with a coherence-dependent filtering that can suppress the accumulation of small-scale phase perturbations. The key consequence is that the *amplitude* of lensing reconstructions (e.g. CMB κ or shear) can be reduced without requiring a commensurate reduction in the clustering amplitude inferred from galaxy density fields at comparable epochs. This leads to a characteristic *redshift-dependent decorrelation*: cross-correlations between lensing maps and density tracers weaken more rapidly with tracer redshift than expected in a purely metric picture.

A convenient way to express this prediction is through ratios that eliminate most dependence on tracer bias and overall power-spectrum normalisation. For a lensing field L (CMB κ or shear) and a galaxy-density tracer g_i in redshift bin i, define the normalised correlation coefficient

$$r_i(\ell) \equiv \frac{C_\ell^{Lg_i}}{\sqrt{C_\ell^{LL}\, C_\ell^{g_i g_i}}}\,. \tag{31}$$

In ΛCDM with standard systematics control, $r_i(\ell)$ is predicted to be close to unity on large angular scales (where stochasticity is small) and to decrease in a controlled manner as nonlinearity and noise increase. ECSM predicts an additional, coherence-driven suppression that becomes stronger as the line-of-sight path length increases and as the kernel overlaps higher-redshift structure, yielding a distinctive scaling:

$$r_i(\ell)\big|_{\rm ECSM} \simeq \mathcal{S}_i(\ell)\, r_i(\ell)\big|_{\Lambda\rm CDM}, \qquad \mathcal{S}_i(\ell) \le 1, \tag{32}$$

with $\mathcal{S}_i$ decreasing with tracer redshift and with multipole once the angular scale probes modes below the effective coherence length. Importantly, this is *not* equivalent to a single global rescaling of A_s or σ_8: a pure amplitude change leaves $r_i(\ell)$ approximately unchanged, whereas ECSM generically predicts a redshift- and scale-dependent reduction.

This decorrelation can be tested with existing data using cross-spectra $C_\ell^{\kappa g_i}$ from CMB lensing reconstructions and tomographic galaxy samples, and analogously with shear-density cross-correlations $C_\ell^{\gamma g_i}$ in weak-lensing surveys. A detection of a systematic trend in $r_i(\ell)$ with increasing tracer redshift (beyond that attributable to known systematics) would provide a sharp discriminator between ECSM and metric interpretations, especially when combined with the peak-position locking and phase-coherent TT/TE/EE signatures discussed above.

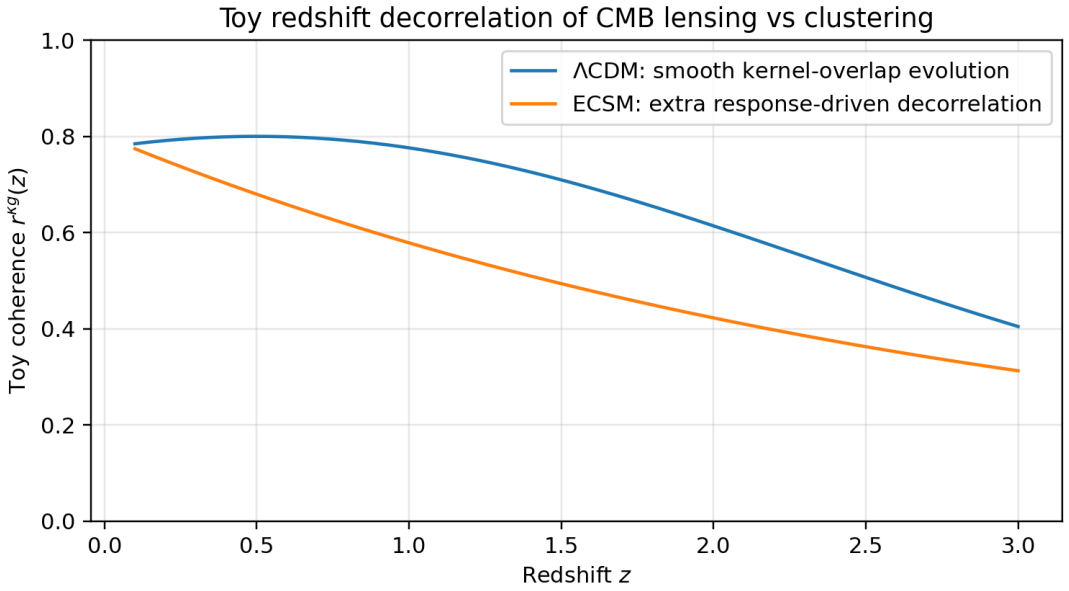

Figure 11: **Toy schematic: redshift decorrelation of lensing versus clustering.** Illustrative behavior of the tomographic coherence $r^{\kappa g}(z)$ (Eq. **??**). In ΛCDM the normalized correlation evolves smoothly with redshift via kernel overlap, while ECSM allows an additional response-driven suppression that accelerates decorrelation with z and cannot be absorbed into a single amplitude parameter.

8.7 Observable: lensing–tracer coherence $r_\ell^{\kappa g_i}$

To quantify how tightly CMB lensing traces a projected matter tracer g_i (e.g. a galaxy overdensity map in tomographic bin i), we use the dimensionless coherence (cross-correlation coefficient)

$$r_\ell^{\kappa g_i} \equiv \frac{C_\ell^{\kappa g_i}}{\sqrt{C_\ell^{\kappa\kappa}\, C_\ell^{g_i g_i}}}, \tag{33}$$

where $C_\ell^{\kappa\kappa}$ is the CMB lensing convergence auto-spectrum, $C_\ell^{g_i g_i}$ is the tracer auto-spectrum, and $C_\ell^{\kappa g_i}$ is their cross-spectrum. By construction, $|r_\ell| \leq 1$ for noiseless fields and common sky coverage.

Map-level estimator. Given HEALPix maps $\kappa(\hat{\mathbf{n}})$ and $g_i(\hat{\mathbf{n}})$ with a common mask $W(\hat{\mathbf{n}})$, we compute pseudo-C_ℓ spectra $\tilde{C}_\ell$ from masked spherical-harmonic coefficients and debias mode-coupling via a coupling matrix $M_{\ell\ell'}$,

$$\hat{C}_\ell^{XY} = \sum_{\ell'} M_{\ell\ell'}^{-1}\, \tilde{C}_{\ell'}^{XY}, \qquad X, Y \in \{\kappa, g_i\}. \tag{34}$$

In practice we bin multipoles into bandpowers b and work with $\hat{C}_b$. Noise biases are removed from auto-spectra by subtracting the corresponding noise (or simulation) spectra, e.g. $\hat{C}_b^{\kappa\kappa} \to \hat{C}_b^{\kappa\kappa} - \hat{N}_b^{\kappa\kappa}$.

Coherence construction. From the debiased bandpowers we form

$$\hat{r}_b^{\kappa g_i} = \frac{\hat{C}_b^{\kappa g_i}}{\sqrt{(\hat{C}_b^{\kappa\kappa} - \hat{N}_b^{\kappa\kappa})\,(\hat{C}_b^{g_i g_i} - \hat{N}_b^{g_i g_i})}}\,. \tag{35}$$

When working directly with published bandpowers (rather than maps), Eq. (35) is applied to the reported $\{C_b^{\kappa g_i}, C_b^{\kappa\kappa}, C_b^{g_i g_i}\}$.

Uncertainties. We estimate $\mathrm{Cov}(C_b)$ and $\sigma(r_b)$ using (i) jackknife resampling over sky regions, and/or (ii) Monte-Carlo suites of CMB lensing reconstructions and tracer mocks with the survey mask and noise properties. The resulting $r_b^{\kappa g_i}$ provides a direct diagnostic of scale-dependent coherence ("redshift decorrelation") between lensing and tracers.

8.8 Redshift-dependent lensing–clustering decorrelation estimator

A direct and model-agnostic probe of the ECSM prediction of lensing–structure decorrelation is provided by the normalized cross-correlation coefficient between the CMB lensing convergence κ and tracers of large-scale structure in a redshift bin i,

$$r_i(\ell) \equiv \frac{C_\ell^{\kappa g_i}}{\sqrt{C_\ell^{\kappa\kappa}\, C_\ell^{g_i g_i}}}. \tag{36}$$

In standard ΛCDM, this quantity is expected to remain approximately constant with redshift at fixed multipole, modulo known geometric and bias effects, since both κ and g_i trace the same underlying matter field. By contrast, in the ECSM framework, lensing efficiency is controlled by the finite induction coherence of the emergent medium, leading to a systematic reduction of $r_i(\ell)$ with increasing redshift even when the clustering amplitude $C_\ell^{g_i g_i}$ remains unchanged.

This estimator is routinely measured by current surveys and does not require any modification to existing analysis pipelines.

8.9 Absence of primordial B-mode polarization

In the ECSM framework, there is no primordial tensor background analogous to that generated by inflationary vacuum fluctuations. As a result, the cosmic microwave background is not expected to exhibit a scale-invariant primordial B-mode polarization component. Any observed B-mode signal must instead arise from secondary effects, including weak lensing leakage from E-modes or local anisotropic response of the emergent medium.

This contrasts sharply with ΛCDM, in which primordial gravitational waves generically source a distinct low-ℓ B-mode spectrum, including a reionization bump and a recombination-scale contribution whose amplitude is parameterized by the tensor-to-scalar ratio r. In ECSM, no such component exists: the polarization field is generated by phase-coherent propagation and quadrupolar response at last interaction, without tensor metric perturbations.

A key prediction of ECSM is therefore that B-mode power should be scale-dependent, strongly suppressed on large angular scales, and tightly correlated with lensing reconstruction or local medium anisotropy indicators. In particular, ECSM predicts the absence of a

clean reionization bump in C_ℓ^{BB} and no detection of a primordial tensor signature even as instrumental sensitivity improves.

Any future detection of a statistically significant, frequency-independent, large-scale B-mode component uncorrelated with lensing or local anisotropy would directly falsify the ECSM framework. Conversely, continued non-detection of primordial B-modes, combined with lensing-consistent BB power, would provide strong support for an intrinsic-medium origin of CMB polarization.

8.10 Absence or strong suppression of primordial B-modes

A third, optional but powerful discriminator concerns primordial tensor B-mode polarization. In the standard inflationary picture, a stochastic background of tensor perturbations generates a primordial BB spectrum with a characteristic large-angular-scale "reionization bump" at low multipoles and a recombination-era contribution at degree scales. In ECSM, we do not posit an inflationary tensor background as the origin of the CMB peak structure; therefore, a natural expectation is that any observed BB signal is dominated by (i) lensing conversion of E-modes into B-modes and (ii) instrument/foreground residuals, with any additional B-mode contribution arising from local or anisotropic medium-response effects rather than from primordial gravitational waves.

This leads to two falsifiable implications. First, if the effective lensing response is suppressed (as suggested by the lensing-amplitude and smoothing diagnostics discussed above), then the lensing-generated BB component should be correspondingly reduced relative to the ΛCDM expectation at the same EE level. Second, absent a primordial tensor contribution, there should be no clean, survey-independent detection of the reionization bump with the standard inflationary shape after delensing and foreground control. Future high-sensitivity polarization experiments can therefore test whether the BB spectrum is fully accounted for by lensing plus contaminants, or whether an irreducible primordial component with the expected inflationary morphology remains.

8.11 Redshift decorrelation of lensing versus clustering

A decisive test of whether the observed lensing-related anomalies arise from late-time structure growth (as in metric cosmology) or from an intrinsic medium response (as in ECSM) is the redshift dependence of lensing–tracer coherence. We propose to measure the cross-correlation coefficient $r_\ell^{\kappa g_i}$ defined in Eq. (**??**) across multiple tomographic redshift bins.

Expectation in ΛCDM. In the standard picture, CMB lensing κ is a line-of-sight projection of the gravitational potential sourced by the same density field that drives galaxy clustering and cosmic shear. Consequently, the normalized coherence $r_\ell^{\kappa g_i}$ is primarily set by kernel overlap and evolves smoothly with redshift: the correlation weakens at very low z (reduced overlap with the broad CMB lensing kernel) and at very high z (reduced tracer signal and increased noise), but does not exhibit a sharp or anomalously rapid loss of coherence at intermediate redshifts once survey systematics are controlled.

Table 3: **Direct observational handles for redshift-dependent lensing–clustering decorrelation.** The key statistic is the tomographic cross-correlation coefficient $r_\ell^{\kappa g_i}$ (Eq. **??**) and closely related ratios using shear γ or CMB polarization-based lensing reconstructions.

Data set	**Observable(s)**	**ECSM-discriminating signature**
Planck (CMB)	κ reconstruction; $C_\ell^{\kappa\kappa}$; $\kappa \times g_i$ cross-correlations (public pipelines exist)	Tomographic $r_\ell^{\kappa g_i}$ shows extra redshift-dependent suppression not captured by global amplitude rescaling; potential scale-dependent decorrelation at high ℓ.
ACT / SPT (CMB)	Higher-ℓ κ reconstructions; polarization-based lensing; consistency across temperature/polarization estimators	Same decorrelation trend persists at higher ℓ (where lensing reconstruction is strongest); consistency between T- and E-based reconstructions disfavors foreground mimicry.
DES / KiDS / HSC (LSS)	Tomographic galaxy density g_i and cosmic shear γ_i; cross with CMB lensing κ	Cross-coherence $r_\ell^{\kappa g_i}$ and/or $r_\ell^{\kappa\gamma_i}$ declines faster with redshift than metric-kernel expectation; decorrelation does not track tracer bias changes alone.
LSST / Euclid (future)	High-S/N tomography in many bins; joint $\kappa \times g_i$, $\kappa \times \gamma_i$, and shear–density cross-checks	High-precision measurement of $r_\ell^{\kappa g_i}(z)$ isolates whether lensing efficiency tracks growth (metric) or exhibits an additional response-driven cutoff (ECSM).

Expectation in ECSM. In ECSM, the mapping between the matter distribution and the effective lensing response is not assumed to be universally metric at all epochs and scales: the observed convergence field can be suppressed by a finite-coherence (or response-screening) mechanism that depends on the medium state along the line of sight. A key consequence is that the *normalized* coherence $r_\ell^{\kappa g_i}$ can fall more rapidly with redshift than in ΛCDM, because the κ–tracer cross-signal inherits an additional response factor that is not shared by the tracer auto-spectrum. In other words, the effective lensing efficiency can partially decouple from the late-time clustering amplitude, producing a redshift-dependent decorrelation that cannot be removed by a single nuisance amplitude such as A_L.

Operational falsifiability. The prediction is falsified if $r_\ell^{\kappa g_i}$ follows the smooth kernel-overlap evolution expected from metric lensing, with no additional decorrelation once survey selection, photometric-redshift uncertainties, and known foreground contaminants are marginalized. Conversely, evidence for an extra suppression of $r_\ell^{\kappa g_i}$ increasing with redshift (and/or with multipole) would support a medium-response contribution to the effective lensing field distinct from late-time clustering.

A Formal Non-Equivalence to Metric Theories

At finite induction coherence length χ, the ray propagation equation derived in this work includes explicit dependence on a nonlocal coherence kernel that suppresses cumulative phase induction along extended lines of sight. Such terms cannot be generated from the Euler–Lagrange equations of any action constructed solely from a Lorentzian metric and its derivatives.

Metric theories require light rays to extremise an integral of the form $\int g_{\mu\nu} k^\mu k^\nu \, d\lambda$, leading to local geodesic equations. By contrast, the induction-modified ray equation involves scale-dependent filtering that violates this variational structure. As a result, no effective metric exists whose null geodesics reproduce the finite-coherence dynamics.

Only in the limit $\chi \to \infty$ does the nonlocal suppression vanish, restoring cumulative induction and allowing an effective metric description to emerge. The theory is therefore intrinsically non-metric except in this singular limit.

B Why This Framework Is Not Modified Gravity

At first glance, any departure from standard gravitational lensing or metric light propagation may appear to fall within the broad class of modified gravity theories. We therefore clarify explicitly why the present framework does not constitute a modification of general relativity, nor a metric theory of gravity.

B.1 No Modification of the Gravitational Field Equations

Modified gravity theories alter the dynamics of spacetime itself, typically by modifying the Einstein–Hilbert action, introducing additional fields, or changing the field equations governing curvature. In contrast, the present framework makes no alteration to gravitational field equations and does not introduce a modified metric sector. No assumption is made regarding the validity or invalidity of Einstein gravity at the level of spacetime dynamics.

Instead, the departure from standard predictions arises solely from the physical mechanism governing light propagation. Gravity remains encoded in the large-scale structure and evolution of the cosmic medium, while geometry emerges only as an effective description in a specific limit.

B.2 Light Does Not Follow Fundamental Geodesics

A defining feature of metric theories is that freely propagating light follows null geodesics of a spacetime metric. In this work, that assumption is explicitly relaxed. Light is treated as an inductive excitation propagating through a condensed cosmic medium, with trajectories determined by local medium response, coherence length, and relaxation properties.

Standard null geodesics are recovered only in the singular limit of infinite induction coherence. At finite coherence, ray paths depend on medium properties rather than on a universal spacetime connection. This places the framework outside the class of metric theories by construction.

B.3 No Additional Degrees of Freedom in the Metric Sector

Many modified gravity models introduce extra scalar, vector, or tensor degrees of freedom that couple directly to matter or curvature. The superfluid ECSM framework introduces no such degrees of freedom in the metric sector. All new structure resides in the response properties of the cosmic medium that governs signal propagation, not in spacetime geometry itself.

Consequently, the framework does not predict fifth forces, violations of local Lorentz invariance in matter dynamics, or departures from standard gravitational motion for massive particles.

B.4 Emergent Geometry Rather Than Altered Geometry

The distinction between modified gravity and emergent geometry is fundamental. Modified gravity alters the rules by which geometry evolves. Emergent geometry questions whether geometry is fundamental at all.

In the present framework, spacetime geometry arises as an effective, coarse-grained description of signal propagation in the limit where induction coherence is large compared to all relevant scales. Outside this limit, geometric notions such as distances, angles, and lensing convergence become scale- and context-dependent observables rather than invariant properties of spacetime.

B.5 Observational Distinguishability

Because the departure from standard predictions originates in propagation rather than gravity, the observational signatures differ qualitatively from those of modified gravity. In particular:

- Weak lensing is suppressed relative to structure growth without altering growth dynamics.
- Convergence and shear decorrelate in a scale- and redshift-dependent manner.
- CMB acoustic features exhibit small, peak-dependent phase shifts rather than uniform rescalings.

These effects cannot be reproduced by modifying gravitational field equations alone and therefore provide a clear observational distinction between emergent-optics models and modified gravity scenarios.

B.6 Survey-specific observational signatures

Planck measurements would primarily detect ECSM signatures through suppressed CMB lensing reconstruction amplitude and mild redshift-dependent decorrelation between κ and low-redshift galaxy surveys, while preserving the acoustic peak positions and temperature–polarization phase structure.

ACT and **SPT**, with higher angular resolution and sensitivity at $\ell \gtrsim 1000$, are particularly well suited to detecting enhanced damping of EE polarization relative to TT, as well as the persistence of peak locking under varying effective lensing strength.

DES and **LSST** cross-correlations with CMB lensing maps provide a direct test of the predicted redshift decorrelation: ECSM predicts a faster decline of $C_\ell^{\kappa g_i}$ with source redshift than allowed by geometric effects alone, even when galaxy clustering amplitudes remain unchanged.

The combination of these datasets enables a decisive test of whether observed lensing anomalies arise from late-time metric effects or from intrinsic medium-induced limitations on phase induction.

B.7 Summary

The framework presented here is not a modification of gravity, but a non-metric theory of light propagation in which spacetime geometry emerges as an effective optical limit. Gravity governs the evolution of the cosmic medium, while observable deviations arise from finite-coherence induction effects. This separation is essential both conceptually and observationally, and places the theory in a distinct class from modified gravity models.

C Recovery of Standard Cosmology in the Infinite-Coherence Limit

The framework developed in this work does not constitute a modification of general relativity or a replacement of the standard cosmological model. Instead, it generalises light propagation by allowing for finite induction coherence in the cosmic medium. In this appendix we demonstrate explicitly that standard metric cosmology is recovered as a well-defined limiting case.

The inductive ray equations derived in Section **??** depend on the coherence scale $\chi_{\rm coh}$, which controls the nonlocal response of the medium to electromagnetic phase perturbations. When $\chi_{\rm coh}$ is finite, ray trajectories depend on the integrated medium response along the line of sight, leading to departures from metric null geodesics. However, in the limit

$$\chi_{\rm coh} \to \infty, \tag{37}$$

the induction response becomes effectively local. Phase perturbations relax instantaneously, and the ray equations reduce to

$$\frac{d^2x^\mu}{d\lambda^2} + \Gamma^\mu_{\alpha\beta}\frac{dx^\alpha}{d\lambda}\frac{dx^\beta}{d\lambda} = 0, \tag{38}$$

corresponding to null geodesic motion in an effective spacetime metric.

In this limit, the convergence and shear fields computed from ray bundles recover their standard gravitational-lensing forms, and the usual relations between lensing, growth of structure, and distance measures are restored. Similarly, CMB acoustic peak positions reduce to those predicted by a single angular-diameter distance to last scattering, with no peak-dependent phase shifts. Any residual scale dependence vanishes as $\chi_{\rm coh} \to \infty$.

Therefore, the ΛCDM cosmology emerges as a controlled limit of the present framework rather than being in conflict with it. Finite-coherence effects introduce additional, physically motivated corrections to light propagation without altering the underlying gravitational dy-

namics. This clarifies that the deviations discussed in the main text represent environment-dependent optical effects rather than violations of metric gravity or energy–momentum conservation.

The existence of this smooth limiting behaviour ensures that the framework is both internally consistent and directly comparable with standard analyses. It also highlights that observational tensions between early- and late-time probes may be interpreted as evidence for finite-coherence propagation rather than as a failure of the standard gravitational description.

D Numerical Robustness and Analysis Stability

This appendix documents the numerical stability and robustness of the peak-phasing and polarization results presented in the main text. The purpose is to demonstrate that the reported signatures do not arise from numerical artefacts, peak-finding bias, or fine-tuned parameter choices.

D.1 Peak Identification and Sub-ℓ Interpolation

Acoustic peak locations in the TT and EE spectra are identified by locating local maxima in the discretized angular power spectra and refining each position using quadratic interpolation over neighbouring multipoles. This sub-ℓ refinement ensures that inferred displacements $\Delta\ell_n$ are not quantized by grid resolution.

For the TE spectrum, phase shifts are measured via the locations of successive zero crossings rather than maxima, providing an independent and less amplitude-sensitive probe of phasing. All reported shifts are therefore geometric in nature and insensitive to overall normalization.

D.2 Planck-Safety Criterion

To ensure consistency with current CMB constraints, we impose a conservative heuristic bound

$$\max_n \left| \frac{\Delta\ell_n}{\ell_n} \right| \lesssim 3 \times 10^{-4}, \tag{39}$$

motivated by Planck sensitivity to acoustic peak locations.

For the transition-phased spectra considered in this work, we find that a representative phase-lag amplitude $\phi_0 \simeq 10^{-3}\,\mathrm{rad}$ satisfies this bound while still producing a clearly peak-dependent displacement pattern. The maximal fractional shifts occur at the lowest acoustic features and decay monotonically with increasing multipole index.

D.3 Parameter Stability

We verified that the qualitative behaviour of the peak displacements is robust under:

- moderate variation of the phase-lag amplitude ϕ_0 within the Planck-safe regime,
- changes in the damping envelope of the toy spectra,
- variation of the peak-identification window size, and

- restriction to $\ell \geq 200$ to exclude low-ℓ non-acoustic structure.

In all cases, the ordering

$$|\Delta\ell/\ell|_{EE} \gtrsim |\Delta\ell/\ell|_{TE} \gtrsim |\Delta\ell/\ell|_{TT} \tag{40}$$

remains intact, confirming that the hierarchy of sensitivities is not an artefact of a particular numerical choice.

D.4 Non-Degeneracy with Distance or Amplitude Rescaling

A uniform angular-diameter rescaling produces $\Delta\ell_n/\ell_n = \text{const}$ across all peaks, while a change in scalar amplitude leaves peak positions unchanged. By contrast, the transition-induced phasing examined here yields a peak-index-dependent displacement pattern that cannot be removed by any single nuisance parameter.

This establishes that the signal is genuinely geometric (in the emergent-optics sense) and not equivalent to a redefinition of standard cosmological parameters.

D.5 Interpretational Scope

The numerical calculations presented here are intentionally minimal and illustrative. They are not intended as a full Boltzmann-code replacement, but as a controlled demonstration that finite transition thickness and finite induction coherence generically imprint correlated, Planck-safe phase shifts across TT, TE, and EE.

A full confrontation with data will require embedding the induction-phase response into a complete polarization transfer calculation. Nevertheless, the existence and structure of the effect demonstrated here are model-independent consequences of finite-depth boundary emission and do not rely on detailed microphysical assumptions.